JOURNAL OF GEOPHYSICAL RESEARCH, VOL. 95, NO. B12, PAGES 19,475–19,493, NOVEMBER 10, 1990

Heat Flow in the Oregon Cascade Range and its Correlation With Regional Gravity, Curie Point Depths, and Geology

DAVID D. BLACKWELL,[1] JOHN L. STEELE,[1] MICHAEL K. FROHME,[2] CHARLES F. MURPHEY,[3] GEORGE R. PRIEST,[4] AND GERALD L. BLACK[4]

New heat flow data for the Oregon Cascade Range are presented and discussed. Heat flow measurements from several deep wells (up to 2500 m deep), as well as extensive new data from industry exploration efforts in the Breitenbush and the Santiam Pass–Belknap/Foley areas are described. The regional heat flow pattern is similar to that discussed previously. The heat flow is about 100 mW m^{-2} in the High Cascade Range and at the eastern edge of the Western Cascade Range. It is about 40–50 mW m^{-2} to the west in the outer arc block of the subduction zone. In the high heat flow zone the heat flow is low at shallow depths in young volcanic rocks due to the high permeability of the rocks and the resultant rapid groundwater flow. Below a depth of 200–400 m much of the area appears to be dominated by conductive heat transfer at least to 2–2.5 km depth. There are perturbations to the regional heat flow in the vicinity of the hot springs where values are up to twice the background. The gravity field in the Cascade Range has characteristics that can be closely related to the heat flow pattern. The relationship may be causal, and to examine the relationship in more detail, earlier two-dimensional modeling is extended to three dimensions. Consideration of the effects of a midcrustal density anomaly, such as might be associated with a region with at least areas of partial melt, has two major consequences. The first of these is that a high-frequency gravity gradient near the Western Cascade Range/High Cascade Range boundary is explained. Second, the negative gravity anomaly associated with the north half of the High Cascade Range can be removed, and as a result, the prominent northeast/southwest striking regional Bouguer gravity anomaly associated with the north edge of the Blue Mountains becomes continuous across the Cascade Range with a similar feature along the north side of the Klamath Mountains. Apparently, this zone is a major crustal feature upon which the negative gravity anomaly coincident with the high heat flow is superimposed. The correlation, or lack thereof, of the heat flow, depth to Curie point, gravity field, crustal electrical resistivity, crustal seismic velocity, and geology in the High/Western Cascade Ranges is summarized. Many of the data show aspects that can be interpreted in relation to possible high temperatures in the midcrust of the Cascade Range. The High Cascade Range midcrust has unusually high temperatures and contains a zone of magma staging at 10 ± 2 km depth that can also be identified in subdued form in the Cascade Range in Washington and British Columbia.

INTRODUCTION

It has become clear in the last 10 years that the coastal provinces of the Pacific Northwest of the United States represent a more typical subduction zone terrain than was initially thought. The 1980 eruptions of Mount St. Helens demonstrated the active volcanism already emphasized by the fact that many of the Cascade Range stratovolcanoes have been active in the last 200 years. Detailed seismic studies have identified clear evidence of a subducting slab under northern California, Oregon, and Washington [*Weaver and Malone*, 1987; *Weaver and Baker*, 1988; *Keach et al.*, 1989]. In addition, evidence has accumulated that large subduction zone earthquakes may also be characteristic of the Pacific Northwest, although perhaps on a time scale more extended than those in areas with faster subduction rates [*Atwater*, 1987; *Heaton and Hartzell*, 1987].

The thermal structure of the crust of volcanic arcs is of great interest but is difficult to obtain because of the non-conductive heat transfer processes that operate there. This complicated nature of heat transfer requires detailed heat flow studies and extensive data coverage. The interest in geothermal energy potential has sparked much study of volcanic arcs, and the thermal characteristics of the Cascade Range volcanic arc are now relatively well known [*Blackwell et al.*, 1978, 1982*a*; *Mase et al.*, 1982; *Lewis et al.*, 1988; *Blackwell et al.*, this issue]. The first objective of this paper is to discuss detailed heat flow data in two areas in the Oregon part of the Cascade Range. This paper starts from the analysis of *Blackwell et al.* [1982*a*], and other background material may be found in that paper.

The second objective of this paper is to compare the heat flow data in central Oregon to other regional geological and geophysical information. In particular, the heat flow pattern is compared to the volcanic patterns and Curie point depths determined by aeromagnetic measurements.

The final objective is to compare in detail the heat flow and gravity fields. Recently, the gravity [*Couch et al.*, 1982*a*, *b*], and magnetic fields [*Couch et al.*, 1985; *Connard et al.*, 1983] of the Cascade Range have been discussed. Also, *Blakely et al.* [1985] combined available gravity and magnetic data in interpreting the tectonic setting of the southern Cascade Range, and in this special section, *Blakely and Jachens* [this issue] discuss the Oregon Cascade Range. In these papers, the heat flow data were not considered of major importance in the interpretation of the gravity data. However, in view of the close correspondence of the thermal and magnetic data it seems appropriate to investigate the correlation of the grav-

[1]Department of Geological Sciences, Southern Methodist University, Dallas, Texas.
[2]Center for Earthquake Research and Information, Memphis State University, Memphis, Tennessee.
[3]Union Pacific Resources, Arlington, Texas.
[4]Department of Geological and Mineral Industries, Portland, Oregon.

Copyright 1990 by the American Geophysical Union.

Paper number 90JB01683.
0148-0227/90/90JB-01683$05.00

ity and heat flow data. The part of the Cascade Range in Washington is discussed in a companion paper [*Blackwell et al.*, this issue].

Summary of tectonics. The tectonic setting of the Oregon Cascade Range is summarized by several papers in this special section [*Priest*, this issue; *Wells*, this issue; *Sherrod and Smith*, this issue; *Stanley et al.*, this issue], and more references may be found in those papers and others in this special section. The details of the subduction of the Juan de Fuca plate are becoming more clear, and the location of the subducting slab has been mapped even in areas with no active seismicity using seismic tomography and electrical studies [*Rasmussen and Humphreys*, 1988; *EMSLAB Group*, 1988; *Booker and Chave*, 1989]. Beneath northern California and the Puget Sound region of Washington the slab is seismically active to depth of up to 80 km [*Ludwin et al.*, 1990]. In Oregon the slab does not appear to be seismically active, although because of the lack of detailed station coverage, small slab earthquakes typical of many seen to the north and the south may not be recorded. All studies show that the slab dips at moderate angles from the trench to the west edge of the Cascade Range. At that point the dip increases abruptly so that the slab is at the typical 100–150 km depths beneath the volcanic arc.

Summary of geology. The primary focus of discussion in this paper is the Western and High Cascade Range provinces (see Figure 1). The Western Cascade Range is a wide belt of volcanic rocks consisting mainly of silicic lavas and tuffs from the early stage (40–18 Ma) and andesitic lavas, dacitic tuffs, and basalts from the middle stages (18–9 Ma) of Cascade arc activity [*Priest et al.*, 1983; *Priest*, this issue; *Taylor*, this issue; *Sherrod and Pickthorn*, 1989]. The High Cascade Range is the center of volcanism within the last 2 m.y. [see *Guffanti and Weaver*, 1988]. This province is dominated topographically by large stratovolcanoes of intermediate composition (e.g., Mount Hood, Three Sisters, Mount Jefferson), although basaltic rocks are volumetrically the dominant rock type. The major volcanoes are identified on the figure. All "identified volcanic systems" and basaltic centers younger than 10,000 years in the area [*Smith and Shaw*, 1975] are also shown.

There are many mapped faults, fault zones, and structural lineaments in and around the Cascade Range. Zones of normal faulting (down to the west) exist on the eastern edge (Green Ridge Fault, Walker Rim) and on the western edge (down to the east) of the High Cascade Range [e.g., *Black et al.*, 1987; *Priest et al.*, 1988]. *Peck et al.* [1964] and *Allen* [1965] suggested that the entire High Cascade Range occupies a broad north-south trending graben. Much of the High Cascade Range is certainly a structural depression even if it is not everywhere bounded by faults.

The Basin and Range province is a geologically complex area, with rocks of all types and ages ranging from Precambrian to Quaternary. This province is currently undergoing extension and is associated with some of the structural features seen in the study area. Within the area of Figure 1, all exposed rocks are volcanics and sediments that are younger than Oligocene.

The High Lava Plains province is characterized by late Cenozoic volcanic and tectonic activity and contains a relatively undeformed sequence of rhyolite domes, young basalt lava flows, silicic ash flows, and cinder cones [*Walker*, 1969]. The Blue Mountains province contains a Mesozoic

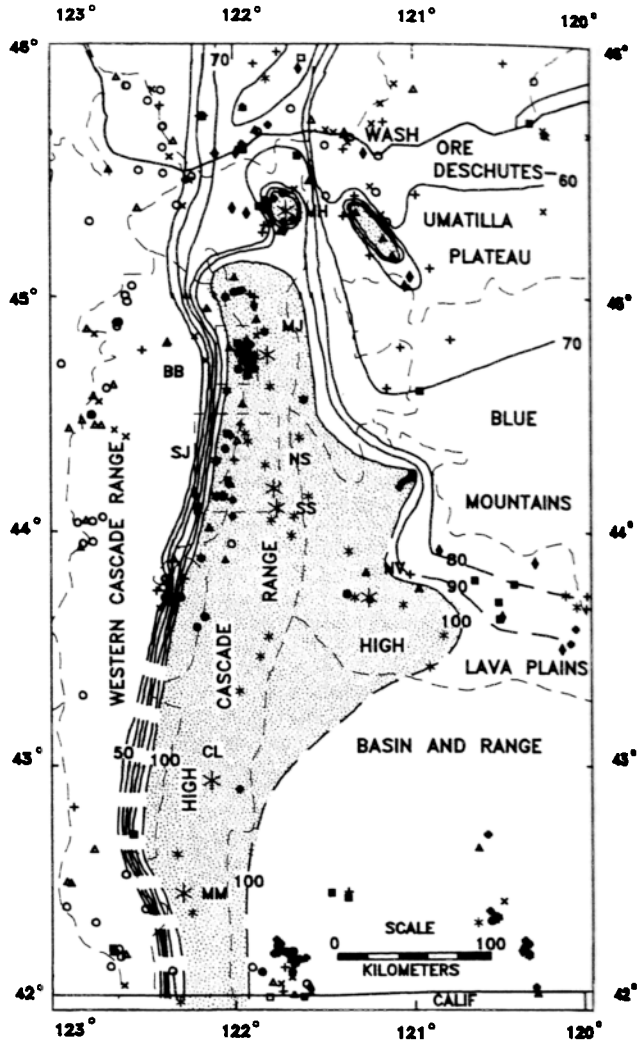

Fig. 1. Heat flow map of central Oregon. Intermediate and large asterisks are young volcanic centers (see text), and dashed lines are physiographic province boundaries. Major volcanoes are Mount Hood (MH), Mount Jefferson (MJ), the Sisters (NS and SS), Newberry volcano (NV), Crater Lake (CL), and Mount McLoughlin (MM). Santiam Junction (SJ) and Breitenbush (BB) areas are indicated by the dashed boxes. Heat flow contours are at 10 mW m^{-2} intervals. Heat flow symbols are open square, 20–30; open triangle, 30–40; open circle, 40–50; cross, 50–60; plus, 60–70; diamond, 70–80; square, 80–90; triangle, 90–100; dot, 100–110; star, 110–120; cross, >120 mW m^{-2}.

basement of sedimentary and intrusive rocks beneath a partial cover of Cenozoic volcanic rocks. Finally, the Deschutes-Umatilla Plateau, occupying the northeast section of the study area, consists of basalts of the Miocene Columbia River group, overlying sedimentary, volcanic, and volcaniclastic units of early to middle Cenozoic.

Summary of geothermal data. The thermal pattern in the Pacific Northwest is clearly that of a subduction zone [*Blackwell*, 1971, 1978, *Blackwell et al.*, 1978, 1982*a*, 1990; *Hyndman*, 1976; *Lewis et al.*, 1985, 1988]. The object of this paper is to summarize thermal results that have become available since the discussion of *Blackwell et al.* [1982*a*] for the Oregon Cascade Range and adjoining provinces, focusing on the volcanic arc. An index map of heat flow is shown in Figure 1 and is used for reference in the following discussion.

Subsequent to the presentation of the thermal data from north central Oregon, regional studies in the United States have been reported for Washington [*Blackwell et al.*, 1985, this issue], for the California Cascade Range [*Mase et al.*, 1982], for the whole Cascade Range [*Blackwell and Steele*, 1983*a*], and for additional data for the Oregon Cascade Range [*Black et al.*, 1983*a*]. Several studies in local areas have increased understanding of the regional data as well. Two of these areas, the Breitenbush and Santiam Junction–Belknap/Foley areas (see Figure 1), are described briefly in this paper.

A detailed study of the Mount Hood volcano (MH in Figure 1) was described by *Steele et al.* [1982] and *Blackwell et al.* [1982*b*]. Holes around Mount Hood are as deep as 1.8 km. In general, the upper parts of the holes, particularly those at high elevation on the volcano, are disturbed by groundwater flow, as is typical of volcanic terrains. However, most of the holes are deep enough to penetrate below this disturbing effect, which typically extends to 200 m or more. The heat flow values measured below the shallow disturbances systematically increase toward the volcanic center, from regional values of 70–80 mW m^{-2} to over 120 mW m^{-2} within 5 km of the center of the volcano. The shape of the anomaly is consistent with a modest subvolcanic magma chamber larger than a volcanic neck but of smaller extent and shallower than the regional heat flow anomaly. This anomaly is shown on the heat flow map in Figure 1.

Williams and Von Herzen [1983] attempted to make heat flow measurements in Crater Lake (CL on Figure 1) using oceanic techniques. Their penetrations were very small, however, and interpretations of heat flow values were made based on penetrations of a few centimeters. These interpreted values show major variations of heat flow. Subsequently, a hole was drilled as part of an exploration project along the western border of the Crater Lake National Park which encountered temperatures of over 100°C with a depth of about 400 m [see *Blackwell and Steele*, 1987] (see 315/7E-10 in Table 1). A controversy has developed over the existence and significance of geothermal systems in Crater Lake [*Sammel and Benson*, 1987].

Near the California border *Black et al.* [1983*b*] described preliminary values for a number of heat flow sites at and around a small geothermal system in the vicinity of Ashland, Oregon (southwest of Mount McLoughlin shown in Figure 1). These measurements are presented in final form in this paper (Figure 1 and Table 1). The Ashland area is part of the outer arc (low heat flow) regional background. In the vicinity of the geothermal anomaly, heat flow reaches maximum values approximately twice the regional background.

Mase et al. [1982] presented extensive data from the California portion of the Cascade Range and in adjoining provinces. Most of their holes were water wells that did not penetrate below the groundwater circulation effects. Consequently, the results provide little regional thermal information in the Cascade Range. Their results document low heat flow in the Klamath Mountains characteristic of an outer arc block. *Beall* [1981] presented temperatures from a well at the southern border of Lassen Volcanic National Park (south of Figure 1) which indicated extremely high temperatures and active fluid flow in a geothermal aquifer. The characteristics of the thermal aquifer in the well have been discussed by *Ziagos and Blackwell* [1986]. This area has since been incorporated within Lassen Volcanic National Park. New temperature data from a deep hole along the Cascade Range crest between Medicine Lake and Mount Shasta are discussed briefly below.

Extensive studies have been carried out at Newberry volcano (NV on Figure 1), near the intersection of the High Lava Plains and the Cascade Range. A hole drilled in 1980 encountered a temperature of 265°C in the crater [*Sammel*, 1981]. Subsequent reports of additional drilling and discussion of the thermal data, and of models, are presented by *Blackwell and Steele* [1983*b*, 1987], *Black et al.* [1984], *Swanberg and Combs* [1986], *Swanberg et al.* [1988], *Sammel et al.* [1988], and others. The most extensive recent discussion of the data is by *Sammel et al.* [1988], and references to other relevant studies can be found in that paper.

HEAT FLOW DISTRIBUTION

Heat flow data. Geothermal gradient, heat flow, and ancillary information for drill holes in the Oregon Cascade Range are summarized in Table 1. Only holes where heat flow is of C quality (see below) or better are included in Table 1. More complete information on the sites in Table 1 is given by *Blackwell et al.* [1989].

Individual holes are located by latitude and longitude and by township and range. Thermal conductivity values are based on measurements on core or cutting samples or are estimated from lithology (values in parentheses). The heat flow values are generally given to the nearest 1 mW m^{-2}, but based on the associated errors of the values, the units place may not be significant. Terrain corrections have been made, if necessary, to the data using the technique of *Blackwell et al.* [1980]. A recent summary of hardware techniques for heat flow studies is given by *Blackwell and Spafford* [1987]. The points in southern Washington are from *Blackwell et al.* [this issue].

There is still a large data gap in the southern Oregon Cascade Range, and the contouring there is preliminary. There are a number of reliable heat flow determinations in the Klamath Mountains and at the south end of the Western Cascade Range indicating typical values for the outer arc, low heat flow province. The details of the heat flow pattern in the provinces east of the Cascade Range are complicated, but the average heat flow is probably typical of the back arc provinces of the Cordillera at 75 ± 10 mW m^{-2} [*Blackwell et al.*, 1990] and so is significantly below that of the Oregon High Cascade Range. Sites of new data from deep holes near Crater Lake, Newberry Volcano, Mount Hood, and Breitenbush hot springs are listed in Table 1 and shown on the map. The new data presented here do not significantly change the heat flow contours described by *Blackwell et al.* [1982*a*] although they add to the details of the pattern, particularly north of Mount Jefferson (MJ in Figure 1).

Two specific areas along the High/Western Cascade Range boundary have a relatively high density of heat flow data, and these areas are discussed in detail in the next two sections to illustrate the observational constraints on the nature of heat transfer in this region. These areas are the Breitenbush hot springs area and the Santiam Junction–Belknap/Foley area (the boxes labeled BB and SJ in Figure 1).

Breitenbush area. The extensive heat flow data in the vicinity of Breitenbush hot springs have been described by *Blackwell and Baker* [1988*a*, *b*]. The data shown on the map

TABLE 1. New Thermal Data for the Oregon Cascade Range and Vicinity

Township/ Range Section	Latitude N, Longitude W	Collar Elevation, m	Depth Range, m	Average Thermal Conductivity, W m^{-1} K^{-1}	SE	N	Corrected Gradient, °C km^{-1}	Corrected Heat Flow, mW m^{-2}	Quality Rating	Lithology Summary
2N/7E 28BDDA	45° 37.67′, 121° 57.17′	18	60–150	1.42	0.17	4	57.1	81	B	andesite
1S/4E 1BCA	45° 30.88′, 122° 15.90′	174	65–150	1.35	0.13	4	35.0	47	B	basalt
1S/4E 10BCA	45° 30.00′, 122° 18.32′	34	20–60	1.49	0.15	4	117.3	174	G	clay and basalt fragments
1S/4E 11ACC	45° 29.90′, 122° 16.70′	46	110–150	1.29	0.13	6	39.3	51	B	basalt
6S/6E 1AA	45° 5.15′, 122° 0.50′	511	100.6–149.4	(1.38)			67.1	92	C	volcanics
6S/7E 29ABA	45° 1.50′, 121° 58.40′	573	0–460	1.67	0.13		140.0	231	G	basalt, pyroclastics
6S/7E 30BBC	45° 1.33′, 122° 0.55′	524	20–297	(1.38)			72.1	100	G	volcanics
6S/7E 26DC	45° 0.75′, 121° 54.90′	673	103.6–121.9	(1.38)			49.7	69	C	volcanics
6S/7E 36DA	45° 0.00′, 121° 53.40′	706	30.4–146.3	(1.38)			48.3	67	C	volcanics
7S/7E 12DC	44° 57.80′, 121° 53.60′	731	82.3–118.9	(1.38)			51.5	71	C	volcanics
8S/1E 9BD	44° 53.47′, 122° 41.63′	338	30–100	(1.38)			33.2	46	C	basalt
8S/8E 28	44° 51.10′, 121° 49.90′	1146	500–1465	1.38	0.06	7	79.8	110	A	basaltic andesite
9S/7E 3CA	44° 49.10′, 121° 56.10′	1219	30–138	(1.38)			67.5	92	C	weathered volcanics
9S/7E 7DDB	44° 48.10′, 121° 59.50′	957	50–150	(1.38)			61.7	84	C	altered tuff
9S/7E 14ACA	44° 47.74′, 121° 54.75′	823	80–360	1.80	0.09		81.4	146	G	basalt and tuff
9S/7E 27ADA	44° 45.99′, 121° 55.70′	828	30–153	(1.38)			67.3	93	C	andesite, basalt, and tuff
9S/7E 29CCB	44° 45.60′, 121° 59.20′	939	70–84	(1.38)			78.0	109	C	basalt and tuff
9S/7E 28CDA	44° 45.55′, 121° 57.55′	823	250–856 0–2457	1.51 1.88	0.14 0.20	5 13	148.0 56.0	222 106	G B	oligocene tuffs
9S/8E 28CCD	44° 45.50′, 121° 57.85′	878	120–153 60–110	(1.38) (1.38)			130.0 172.5	180 238	G G	soft grey clay
9S/7E 34DBB	44° 44.95′, 121° 56.20′	939	20–150	(1.38)			96.2	130	G	basalt and basalt
9S/7E 36BAD	44° 44.80′, 121° 53.60′	895	50–154	(1.38)			77.3	107	C	altered basalt and andesite
10S/7E 9BBC	44° 43.55′, 121° 57.95′	1329	10–152	(1.38)			99.9	138	G	basalt and basalt andesite
10S/7E 23BCB	44° 41.60′, 121° 55.55′	817	85–152	(1.38)			84.2	117	C	basalt and basalt andesite
10S/7E 24ACB	44° 41.60′, 121° 53.65′	975	50–145	(1.38)			78.9	109	C	andesite, dacite
10S/7E 20CBB	44° 41.45′, 121° 59.20′	640	75–153	(1.38)			78.4	108	C	welded tuff
10S/7E 34ACA	44° 39.90′, 121° 55.95′	780	50–150	(1.38)			71.8	100	C	andesite basalt andesite
12S/9E 1BCD	44° 33.70′, 121° 36.42′	999	35–105 70–105	1.55 1.55	0.21 0.21	4 4	70.0 75.0	108 116	C C	tuff, conglomerate basalt
13S/7E 9CB	44° 27.25′, 121° 58.62′	501	107–149	(1.59)			43.8	69	C	volcanics
13S/6E 26BA	44° 25.00′, 122° 3.60′	1226	126.7–163.3	(1.38)			60.4	83	C	andesite
13S/6E 25AC	44° 24.50′, 122° 2.13′	973	40–143	1.74			99.5	173	G	basaltic andesite
14S/6E 15AD	44° 21.20′, 122° 4.20′	1280	125–155 60–125	(1.38) (1.38)			124.2 78.4	169 107	C C	volcanics
14S/7E 31DD	44° 18.25′, 122° 0.80′	960	150–166.7	(1.59)			42.0	67	C	volcanics
15S/15E 30AA	44° 14.67′, 120° 58.05′	989	25–118	1.65		1	66.0	109	C	claystone
15S/6E 35	44° 13.12′, 122° 3.03′	754	122–154	(1.59)			50.7	80	C	basaltic andesite
16S/6E 1BC	44° 12.18′, 122° 2.09′	535	9–146	(1.72)			53.3	92	C	andesite
16S/6E 21CA	44° 9.30′, 122° 5.30′,	657	73–137	(1.59)			73.1	116	C	andesite basalt

TABLE 1. (continued)

Township/ Range Section	Latitude N, Longitude W	Collar Elevation, m	Depth Range, m	Average Thermal Conductivity, W m^{-1} K^{-1}	SE	N	Corrected Gradient, °C km^{-1}	Corrected Heat Flow, mW m^{-2}	Quality Rating	Lithology Summary
16S/6E 30AD	44° 8.90′, 122° 7.40′	666	50–167	(1.38)			81.8	113	C	volcanics
16S/6E 36AB	44° 8.15′, 122° 1.36′	900	91–235	(1.59)			78.0	124	C	andesite basalt
20S/12E 24BCB	43° 49.50′, 121° 14.82′	1786	1174–1220	1.80			53.2	96	C	basalt and rhyolite tuff
21S/3E 17DA	43° 44.80′, 122° 28.25′	360	70–240 240–340	1.82 1.84			40.5 36.0	74 66	B B	mudstone and siltstone
21S/3E 26CAA	43° 43.07′, 122° 25.17′	427	30–160	1.55			31.3	49	B	silicified volcanics
21S/13E 31CC	43° 42.50′, 121° 13.50′	1943	660–930	(1.46)			999.0	1594	G	tuff, sedimentary basalt
22S/4E 6ADD	43° 41.45′, 122° 22.38′	488	7–155	(1.38)			91.0	126	G	volcanics
22S/12E 25BD	43° 38.25′, 121° 14.45′	1754	1146–1226	1.80			83.7	151	G	basalt and rhyolite tuff
26S/2W 23AAD	43° 17.83′, 122° 53.49′	289	30–52	(1.59)			27.0	43	C	basalt
27S/5W 23AA	43° 12.78′, 123° 14.83′	195	20–64	(1.59)			14.8	23	C	eocene basalt
31S/7E 10	42° 53.85′, 121° 59.25′	1859	0–405	(1.92)			250.0	481	G	andesite
33S/2E 17ADC	42° 42.15′, 122° 36.02′	683	55–130	1.55	0.03	4	60.5	94	B	basalt
33S/2E 17ADD	42° 42.08′, 122°35.88′,	597	60–92.5	(1.55)			53.5	83	C	basalt
33S/18E 23CBD	42° 41.65′ 120° 34.09′	1372	10–233	(1.26)			314.8	395	G	
34S/1W 4DDC	42° 38.26′, 122° 49.22′	491	100–212.5	(1.59)			22.3	38	C	basalt and andesite
36S/11E 14AAA	42° 27.33′, 121° 22.20′	1317	0–354 354–425	(1.59)			34.5 39.9	64	B B	Yonna formation basalt
36S/11E 13ACC	42° 27.07′, 121° 28.03′	1318	5–65 5–100	(1.00)			112.1 82.5	83	C C	Yonna formation
36S/11E 23DCA	42° 25.80′, 121° 22.37′	1316	10–35 35–50	(1.00)			147.0 86.8	87	C C	Yonna formation
37S/2E 4ADD	42° 22.93′, 122° 31.86′	561	40–96.5	1.45			(28.0)	41	C	basalt
38S/9E 28DAB	42° 14.03′, 121° 45.36′	1289	50–115 115–233	(1.00) (1.59)				285	G G	sediment, basalt
38S/9E 32DAA	42° 13.17′, 121° 46.60′	1247	0–629	(1.26)			(300.0)	377	G	sediments, basalt
38S/1E 31DAD	42° 13.13′, 122° 44.28′	505	70–105	1.87	0.15	3	50.7	95	G	shale and diorite
39S/1E 4BBD	42° 12.74′, 122° 42.76′	536	20–330	(1.88)			44.6	84	G	sediments and granite
39S/1E 2BCB	42° 12.65′, 122° 40.57′	622	50–177.5	(1.88)			23.9	45	C	fine silt and sands
39S/1E 4CDD	42° 12.05′, 122° 42.52′	502	5–152.5	1.81	0.21	6	54.0	97	G	shale and granite
39S/1E 10BCB	42° 11.70′, 122° 41.82′	573	60–153	1.78	0.21	4	29.3	51	B	shale
39S/1E 10CDB	42° 11.25′, 122° 41.45′	603	65–122.5	1.75	0.21	7	24.2	42	B	shale
39S/1E 14DBB	42° 10.62′, 122° 40.07′	635	95–150	1.66	0.21	2	27.0	45	C	sandstone to 112 shale to 150
39S/1E 15CDB	42° 10.42′, 122° 41.33′	731	50–212.5	(3.05)			16.6	514	C	granite
40S/4E 5DB	42° 7.08′, 122° 22.50°	1055	10–46 46–99	1.23 1.23	0.04 0.04	8 8	27.4 36.7	34 45	B B	basalt andesite
41S/9W 15CCC	42° 0.10°, 123° 45.30′	897	130–205	2.25	0.41		13.0	29	C	quartz diorite

The section location is subdivided into quarters where a designation 12 ABCD indicates a well in the SE 1/4 of the SW 1/4 of the NW 1/4 of the NE 1/4 of section 12. SE is the standard error of the mean. Parentheses around the thermal conductivity value signify values estimated from surrounding wells or lithology. *N* is the number of thermal conductivity samples. The gradients have all been corrected for topographic effects where necessary. The statistical errors of the heat flow values are usually small so an estimate of the error is given as a quality ratings of A (±5%), B (±10%), C (±25%), and G (geothermal system value, no error implied). Various data points as described in text are from *Black et al.* [1983*b*], *Blackwell and Baker* [1988*a*, *b*], and *Blackwell and Steele* [1987]. More details for each site (including hole name, uncorrected gradient, etc., are given by *Blackwell et al.* [1989].

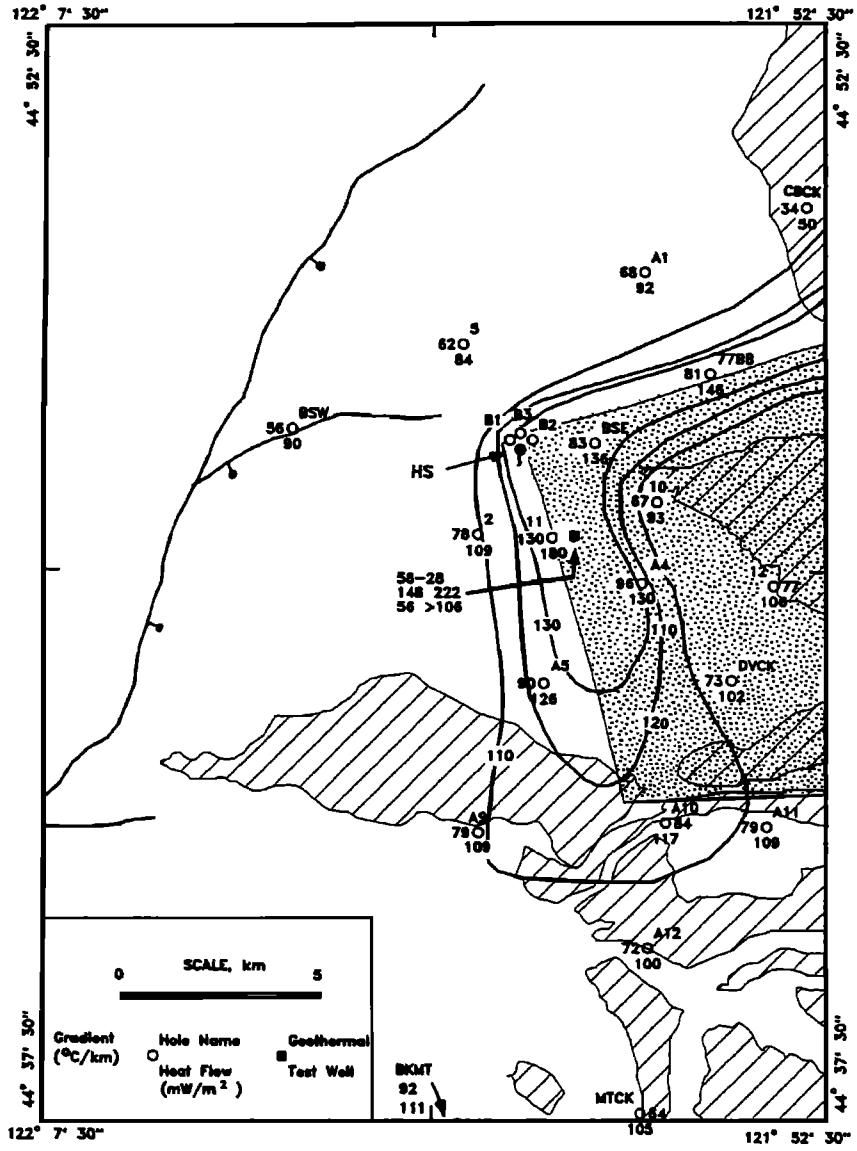

Fig. 2. Map showing heat flow sites, geothermal gradients, and heat flow in the vicinity of Breitenbush hot springs. Heat flow contours within the anomaly are shown for 110, 120, and 130 mW m^{-2}. Rocks younger than about 2 Ma are shown by the diagonal line pattern. Geologic contacts and faults (heavy lines) are from *Priest et al.* [1987]. Dot pattern indicates the extent of the geothermal aquifer as inferred from heat flow and geothermal gradient data.

in Figure 2 (the BB box on Figure 1) include one well 2.5 km deep (Sunedco Federal 58-28, FED 58-28), 19 holes about 150 m deep, and two holes of intermediate depth (B2 and 77BB). All the heat flow data are listed in Table 1 or are from *Blackwell et al.* [1982*a*]. Temperature-depth data from the twelve 150-m holes drilled by Sunedco for geothermal exploration are shown in Figure 3, and the temperature-depth data for the deep well are shown in Figure 4. All of the shallow and intermediate depth wells, with one exception (CBCK, [*Blackwell et al.*, 1982*a*]), were drilled in rocks older 2 Ma, and all have essentially constant gradients that exceed 50°C km^{-1}.

A distinct local geothermal anomaly is associated with the hot springs and can be distinguished from the regional background values of 65 ± 5°C km^{-1} and 100 ± 10 mW m^{-2}. The anomaly is dominated by steep horizontal gradients of heat flow that suggest that the system is dominated by flow along steep fracture systems, at least to a depth of 1 km or so. As discussed below, one component of the system may be an aquifer near the top of the Oligocene Breitenbush Formation.

The shape of the temperature-depth curve for the deep well, FED 58-28, is peculiar (Figure 4). The temperature increases rapidly with a gradient of 148°C km^{-1} to reach a temperature of 116°C at 800 m. Below this depth, the temperature gradient is very low, with a gradual increase to about 30°C km^{-1} at 1700 m. The bottom part of the hole had filled with mud, so the logging tool did not penetrate to the total depth of the hole (2457 m). The only bottom-hole temperature data available are a series of maximum-thermometer runs. A maximum temperature of 141°C was measured 25 hours after the hole had been completed.

The bottom-hole temperature data do not allow a simple extrapolation to equilibrium, but a bottom-hole temperature

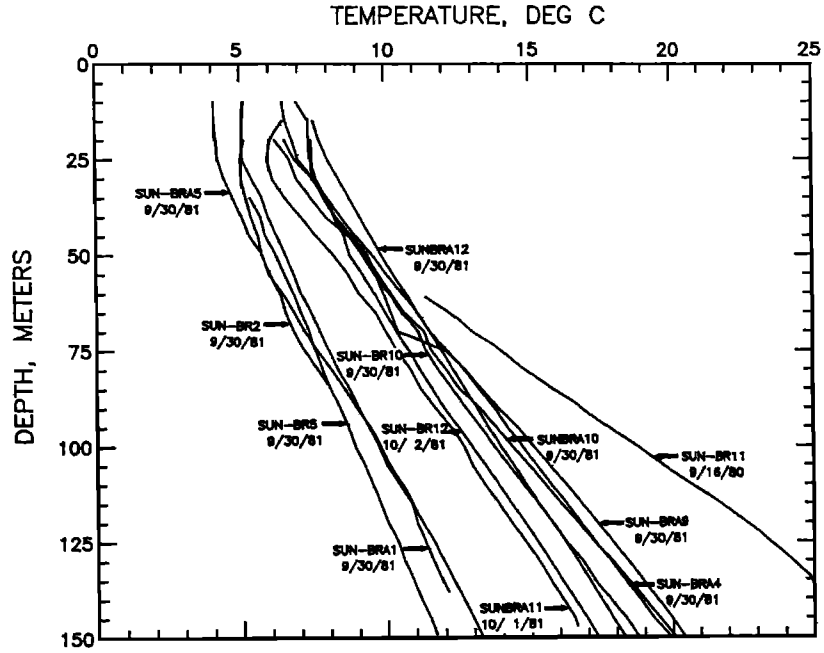

Fig. 3. Temperature-depth plots from Sunedco 150-m deep holes. Temperatures were measured every 5 m. Numbers correspond to Figure 2 except that the SUN-BR has been left off of the site identifications.

of about 150°C is conservative. If the bottom-hole temperature is assumed to be about 150°C, and it is assumed that the temperature at the bottom is not raised too much by the effect of the fluid flow in the aquifer at 780 m, the average temperature gradient between the surface temperature and the bottom of the hole would be about 50°C km^{-1} (the dash-dotted line in Figure 4). The temperature-depth result is very close to the curve observed in the Old Maid Flat hole (OMF-7A; see Figure 4) a 1837-m-deep geothermal gradient hole about 10 km west of Mount Hood, the second deepest hole in the High Cascade Range. A conductive temperature gradient for FED 58-28 would be expected to decrease with depth, because it is drilled in a topographically low area relative to surrounding terrain (negative topographic effect). In addition, thermal conductivity increases 50% with depth (see Table 1, the temperature effect on thermal conductivity is included), so that the geothermal gradient should decrease significantly between the surface and 2.5 km even if no disturbing influences were present. For the depth interval from 0 to 2457 m, ignoring the assumed disturbance from the

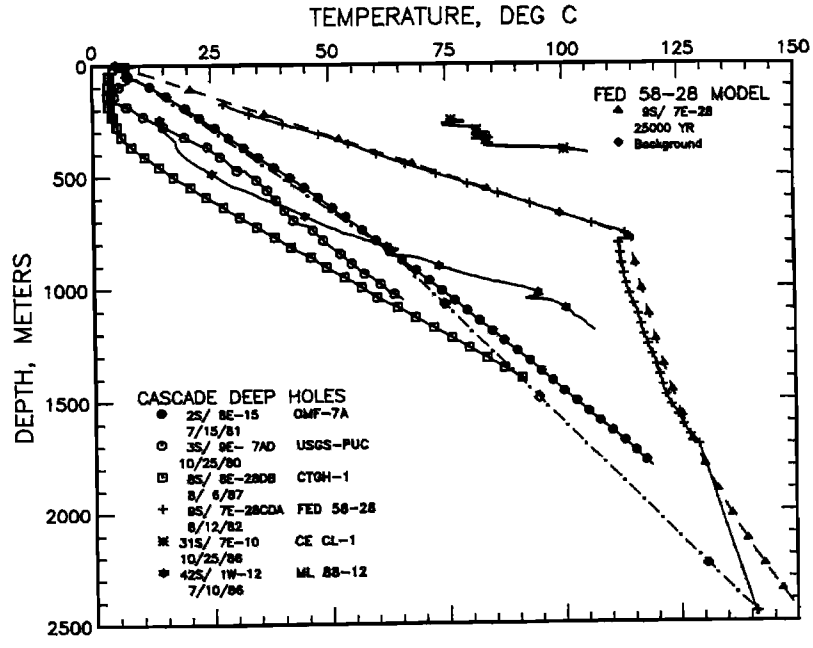

Fig. 4. Temperature-depth curves for deep wells in the Cascade Range. Township and range locations, names, and dates of logging are given. Every ninth point on each curve is shown by a symbol. The assumed background and calculated aquifer model temperature-depth curves for FED 58-28 are the dash-dotted and dashed lines, respectively.

TABLE 2. Thermal Characteristics of the Breitenbush Hot Springs and Geothermal System, and Parameters Used for the Aquifer Model

Parameter	Value
Flow volume, L s^{-1}	57
Spring temperature*, °C	92
Reservoir temperature*, °C	195
Sulfate geothermometer*	181
Total heat loss (T_0 = 10°C), W	4.4×10^7
Convective heat loss, W	2.2×10^7
Conductive heat loss, W	2.2×10^7
Area to generate heat, km^2	440
Area of anomalous heat flow, km^2	110–220
Aquifer thickness, m	30
Flow velocity, m yr^{-1}	
Aquifer width 4 km with 15% porosity	9.9
Aquifer width 6 km with 25% porosty	4.0
Averge thermal conductivity, W m^{-1} K^{-1}	
0–800 m	1.53
800–250 m	2.30
Flow parameter† $\alpha = K_r/VMC$	0.38–0.25

After *Blackwell and Baker* [1988*a*, *b*].
*Temperatures from *Brook et al.* [1979]
†K_r is rock thermal conductivity, V is fluid velocity, M is mass per area of fluid in the aquifer, and C is fluid heat capacity.

aquifer, the measured, temperature-corrected thermal conductivity is 1.88 W m^{-1} K^{-1}, the mean gradient is 56°C km^{-1}, and the heat flow is 106 mW m^{-2} (Table 1). Therefore the bottom-hole temperature, the average geothermal gradient, and the heat flow are equal to the regional values that occur outside the geothermal anomaly, and we infer that the aquifer anomaly is represented by the area between the dash-dotted and the dashed lines in Figure 4.

In contrast, the heat flow value of 222 mW m^{-2} observed above 800 m and the temperature at 800 m in FEDCO 58-28 are definitely anomalous with respect to the regional values. The high values are explained by geothermal fluid in an aquifer located at about 780–800 m that has introduced a transient temperature anomaly. The aquifer, a porous tuff unit, was recognized during drilling (A. Waibel, personal communication, 1987) and has been mapped in outcrop at the hot springs [*Priest et al.*, 1987]. Thus the high temperatures in the well and at the springs are associated with geothermal fluid in an aquifer that intersects the surface in the topographically low area near the springs.

If the flow in the vicinity of the hole is confined to a stratigraphically controlled thermal aquifer, the factors controlling the shape of the temperature-depth curve are analogous to those described for wells in the Long Valley caldera, California [*Blackwell*, [1985]. However, unlike the Long Valley situation, there is only a limited amount of information available for the geothermal aquifer at Breitenbush hot springs. Using known and assumed parameters for the geothermal aquifer as shown in Table 2, *Blackwell and Baker* [1988*a*, *b*] modeled the aquifer temperatures by the technique of *Ziagos and Blackwell* [1986] as applied by *Blackwell* [1985] to the Long Valley geothermal system. The results are shown in Figure 4. The best fitting model (shown by the dashed line) assumes a mean background gradient of 54°C km^{-1} and an age of about 25,000 years for flow through the aquifer. Because of the uncertain bottom-hole temperature, *Blackwell and Baker* [1988*a*, *b*] did not attempt a perfect match to the observed temperatures.

Ingebritsen et al. [1989] used the observed gradient between 1465 and 1715 m in FED 58-28 to infer a background gradient and heat flow of 31°C km^{-1} and 68 mW m^{-2}, respectively, for the well. In this case the heating from the aquifer must raise the temperature at 2500 m by at least 70°C, and the age of flow in the aquifer must be measured in the hundred thousands of years. For a background gradient of 31°C km^{-1}, the heat flow is 71 mW m^{-2} because the temperature corrected thermal conductivity in the welded tuffs in the bottom of the hole is 2.3 W m^{-1} K^{-1}.

The model for the Breitenbush geothermal system based on the analysis of *Blackwell and Baker* [1988*a*, *b*] as described in this section involves relatively slow flow of geothermal fluid from a recharge point in the High Cascade Range to the hot springs. In the area immediately south and east of the hot springs the geothermal fluid flows through a thin aquifer in the Oligocene Breitenbush Formation. The north and west margins of the flow system are defined by intersections of the aquifer and two fracture systems. The fracture systems are conduits for upward fluid leakage from the aquifer. The two fracture systems, the aquifer and the surface, intersect at the hot springs resulting in the escape of fluid to the surface. The geothermal system has been in existence for at least several ten thousands of years. Areas outside the hot springs anomaly have regional heat flow values of 100 ± 10 mW m^{-2}.

Santiam Junction–Belknap/Foley Area. There is an extensive new data set available in the area between Santiam Junction and Belknap/Foley hot springs, approximately 44°30′ to 44°10′N (Figure 1, box labeled SJ). Locations of drill holes with geothermal gradients and heat flow values are shown in Figure 5. The new holes (Table 1) were drilled for geothermal exploration, and thermal conductivity samples were not available for measurement; therefore thermal conductivities were estimated from lithology. Since there are a number of nearby holes with thermal conductivity data [*Blackwell et al.*, 1982*a*] and since the thermal conductivity in the volcanic rocks does not vary much, these estimates probably result in reasonably reliable values of heat flow. This area has a complex thermal pattern. Heat flow in 150-m holes is zero to negative on the east side, increases to quite high values in the center of the map, and then decreases west of the map area to values of less than 60 mW m^{-2}. This same regional pattern is observed elsewhere in the Cascade Range [*Blackwell et al.*, 1978, 1982*a*].

The geology of the area is shown in a very simplified form in Figure 5 [from *Priest et al.*, 1988; *Black et al.*, 1987]. The western part of the area is underlain by Pliocene and older volcanic rocks, whereas the eastern part of the area is covered by Quaternary volcanic rocks. A series of down-to-the-east normal faults representing the west side of the Cascade graben divides the two areas. Most of the area of young rocks west of the crest and north of 44°10′N is covered by a series of basalt flows that are about 3000 years old [*Taylor*, 1968]. Drill holes 150 m deep in the young rocks are isothermal due to the rapid lateral flow of groundwater. At slightly greater depths, or in older rocks, the lower permeability decreases overall fluid flow velocity and limits the flow to discrete zones such as fractures, and the heat transfer is both conductive and convective.

Two histogram sets are shown in Figure 6 to illustrate the

characteristics of the gradient distributions along the boundary of the High and Western Cascade Ranges. In Figure 6, gradient histograms are shown for the wells in Figures 2 and 5. For the Santiam Junction–Belknap/Foley springs area the gradients are grouped into in three categories based on the geology and topographic setting; Quaternary rocks at high elevation; Quaternary rocks at low elevation; and all rocks older than Quaternary. The mean gradient for the first set of data is negative, and the mean gradient for the second set of data is about 25°C km^{-1}, except for gradients exceeding 100°C km^{-1} in two wells that are probably associated with the flow of warm water. Temperature gradients in volcanic rocks older than Quaternary range from 50° to 82°C km^{-1}, and the mean gradient in this group of wells is 67 ± 4°C km^{-1} (N = 10).

In one hole (13S/7E-32DC [*Blackwell et al.*, 1982*a*], Figure 6) the geothermal gradients range from 26°C km^{-1} (0–560 m) to 112°C km^{-1} (15–200 m). The shape of the temperature-depth curve clearly indicates lateral flow of warm water in a confined aquifer through an area otherwise characterized by a lower-than-background heat flow related to deep recharge. A 150-m well 4 km to the northeast has a gradient of 100°C km^{-1} (13S/6E-25AC), the highest gradient along the boundary province not near a known geothermal anomaly. Consequently, in the northern part of the map (stippled area on Figure 5) there is probably lateral flow of warm water at relatively shallow depth.

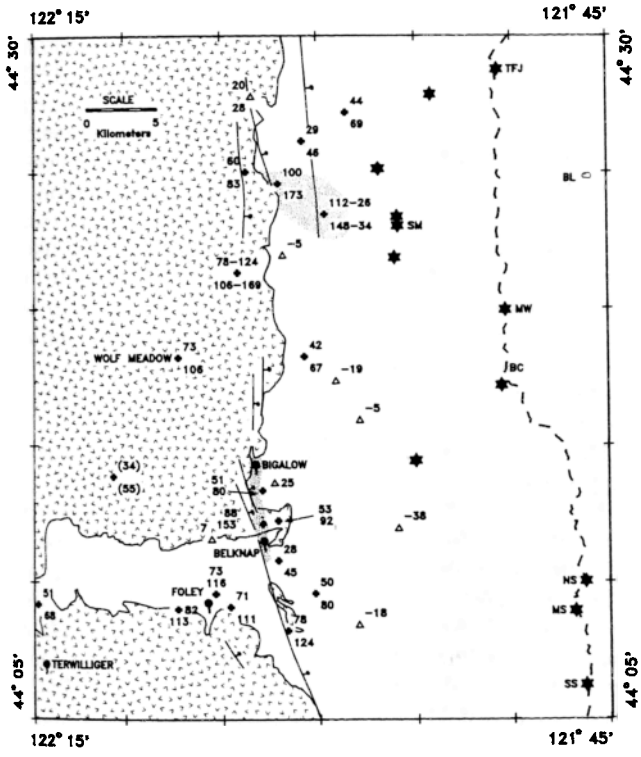

Fig. 5. Geothermal gradient (°C km^{-1}, upper value) and heat flow values (mW m^{-2}, lower value) for sites in Santiam Junction–Belknap/Foley area. Holes in Holocene rocks are marked by open triangles. Major volcanic centers are shown as stars; Cascade Range crest is the dashed line. Major west edge bounding faults of Cascade graben are shown. Rocks older than Quaternary shown by the caret pattern [from *Black et al.*, 1987; *Priest et al.*, 1988]. Stippled pattern marks larger areas of fluid flow and heat flow anomalies. Abbreviations are TFJ, Three Finger Jack; BL, Blue Lake; MW, Mt. Washington; BC, Belknap Crater; NS, MS, SS; North, Middle and South Sister; SM, Sand Mountain.

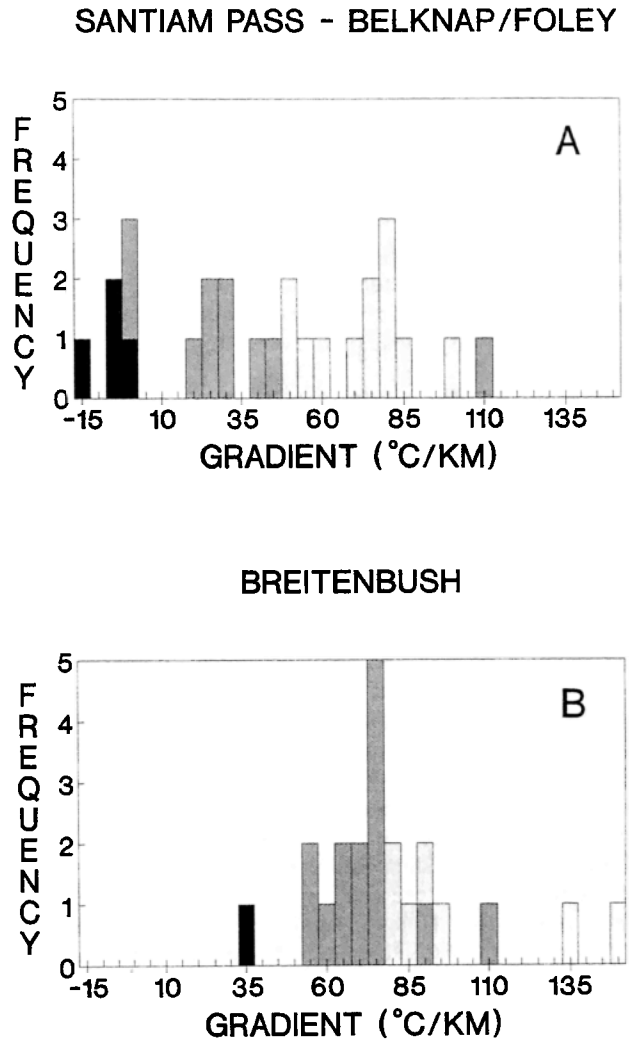

Fig. 6. (*a*) Histograms of geothermal gradient for Santiam Junction–Belknap/Foley area. Gradients in Quaternary rocks at high elevations are solid blocks, in Quaternary rocks at low elevations have a diagonal ruling, and in pre-Quaternary rocks are stippled. (*b*) Histograms of geothermal gradient for Breitenbush area. Gradients outside the geothermal system are indicated by the hatched pattern and those inside the geothermal system are indicated by the stippled pattern. The only hole not in pre-Quaternary rocks is indicated by solid pattern.

The gradients from wells in the Breitenbush area in Figure 6 are coded based on whether or not they occur in the geothermal anomaly associated with the hot springs. Clearly, the cutoff point is arbitrary because the heat flow anomaly blends with the background. If the gradients definitely associated with the thermal anomaly are not included, the average geothermal gradient is 72° ± 4°C km^{-1} (N = 9).

The geothermal model for the Santiam Junction–Belknap/Foley area is considerably more complicated than the one for the Breitenbush area. There is significant fluid flow at depth in the Quaternary rocks of the Cascade graben (the eastern half of Figure 5), in some cases confined to discrete aquifers and in others as general porous media flow. The flow systems are terminated against the low-permeability rocks of the Western Cascade Range and warm water comes

to, or close to, the surface along the faults bounding the graben. The depth of flow cannot be established at the present time because there are no drill data available below 400 m. The leakage of geothermal fluid into the McKenzie River can be accounted for by the less than spectacular flow of Belknap and Foley hot springs [*Mariner et al.*, this issue], so there is not evidence for major fluid flow associated with the systems that cause the high heat flow observed along the fault zone. The inferred reservoir temperatures of the Belknap and Foley systems are only 113° and 99°C, respectively [*Brook et al.*, 1979], temperatures that could be reached at depths of less than 2 km with a regional gradient of 66°C km^{-1}.

Regional thermal characteristics. For comparison to the Breitenbush and Santiam Junction–Belknap/Foley areas the average geothermal gradient along the High/Western Cascade Range boundary between 43°30′ and 45°15′N is 66° ± 4°C km^{-1} [*Blackwell et al.*, 1982*a*, Table 2]. So even though both areas are characterized by the presence of local high heat flow associated with geothermal anomalies, the average gradients in rocks greater than 2 Ma outside the anomalies are similar statistically to regional values. In addition, in these areas high gradients and heat flow values are observed at high elevation as well as low elevation with the reverse also being true. This point is further illustrated by the Wolf Meadow hole, one of the westernmost holes in Figure 5 showing high gradient. This hole has a collar elevation of over 999 m and a geothermal gradient of 73°C km^{-1}. It is well to the west of the set of down-to-the-east Cascade Range graben-bounding faults along the McKenzie River, about 500 m above the river, and is drilled in an impermeable, altered tuff. Holes in similar settings are found from 43°30′ to 45°15′N (for example, BKMT on Figure 2). It is very difficult to understand how regional groundwater circulation could explain such consistently high values of gradient, at such high elevations, so far west of the bounding structures associated with the permeable, young volcanic rocks in the High Cascade range. As a result, the simple gravity driven hydrology pattern proposed by *Ingebritsen et al.* [1989] cannot easily be invoked to explain the regional distribution of gradients and heat flow values in the Western Cascade Range.

The gradient pattern illustrated using the data in Figure 6 has been previously described by *Blackwell et al.* [1982*a*]. They concluded from the drilling evidence that the shallow hydrologic properties and shallow thermal conditions were related to degree of rock alteration, which coincides to some extent with maximum depth of burial (maximum temperature reached) of the rocks. The effect of alteration on decreasing permeability and suppressing any surficial groundwater flow is very clear in the Breitenbush area [*Blackwell and Baker*, 1988*a*, *b*]. The degree of success of obtaining gradients in 150-m holes in the Cascade Range described by *Blackwell et al.* [1982*a*] is a testimony to the careful selection of sites based on age and alteration criteria by the DOGAMI geologists in charge of siting the wells. The geothermal exploration studies, which have been more constrained by a need to have data from certain locations and/or characterized by lack of attention to the local geology, have had significantly lower rates of success in 150-m exploration holes as illustrated by the exploration data shown in Figure 5 and the histograms in Figure 6.

The extensive fluid flow at shallow depths has been referred to as the "rain curtain" and discussed in detail for two Newberry Volcano holes by *Swanberg and Combs* [1986] and *Swanberg et al.* [1988]. As a further contribution to the discussion of the deep significance of temperature gradients in 150-m holes, temperatures from deep holes in the Cascade Range are shown in Figure 4 (see also Figure 3 of *Blackwell et al.* [1982*a*]). All holes in excess of 1 km are plotted, excluding data from the Newberry volcano (which show similar characteristics). The two holes near Mount Hood are included. In all cases the gradients and heat flow values in the deep holes are consistent with the predictions based on 150-m holes nearby or on regional considerations.

Hole CTGH-1 shown in Figure 4 was drilled near the Cascade Range crest north of Mount Jefferson (the star just east of the east border of the BB box). It has a heat flow of 110 mW m^{-2} (see Table 1). Its thermal characteristics have been discussed in detail by *Blackwell and Steele* [1987] and *Blackwell and Baker* [1988*a*, *b*]. The increase in gradient to regional values below 400 m is associated with the presence of alteration that has occurred at temperatures above 50°C [*Barger*, 1988].

Also shown in Figure 4 are temperature-depth curves from a well at the edge of Crater Lake Park (CE-CL-1) in an area of no surface geothermal manifestations, a deep hole drilled by an exploration company approximately midway between Mount Shasta and Medicine Lake (ML-88-12), and a deep hole close to the apex of Mount Hood and much higher in elevation than OMF-7a (USGS-PUC). ML-88-12 is at high elevation in the region of zero to negative surface geothermal gradients based on shallow hole data [*Mase et al.*, 1982]. ML-88-12, CTGH-1, and USGS-PUC show the characteristics of deep holes in the High Cascade Range of low gradient to a depth of 200–500 m and high gradients below that depth. The temperatures in ML-88-12 are not at equilibrium as indicated by hooks in the temperature-depth curve. However, the mean gradient between 500 m and 1.2 km is 100°C km^{-1} and at a depth of 1.2 km the temperature is over 105°C. Hole CE-CL-1 has a high gradient (about 250°C km^{-1} based on a nonequilibrium log). It illustrates that if the surface rocks are altered, gradients may be obtained even above the depth of 200–400 m typical of areas with unaltered rocks at the surface.

These results show that isothermal sections occur to depths ranging up to 400 m at various sites within the Cascade Range. It also shows that, on the basis of present data, consistently high geothermal gradients (in excess of 50°C km^{-1}) are observed below the zone of shallow groundwater circulation. Furthermore, there is often an abrupt depth transition between rocks which have high permeability and rapid fluid through-flow (near isothermal temperature-depth curves) and rocks where the average permeability is quite low and fluid flow is suppressed. The 50- to 200-m transition zones from low to regional values of geothermal gradient typical of the deep holes is evidence that large-scale flow at depth is unlikely except along particularly favorable stratigraphic regions (such as between 780 and 800 m in Sunedco 58-28) or along fractures or fault zones. With the exception of the hole near Santiam Junction shown on Figure 5 (13S/7E-32DC) all holes over 300 m deep in the high heat flow region have gradients below surficial water flow disturbances of over 50°C km^{-1}.

Nonetheless, geothermal fluid circulation plays a role in heat transfer in the High Cascade Range. The models of heat

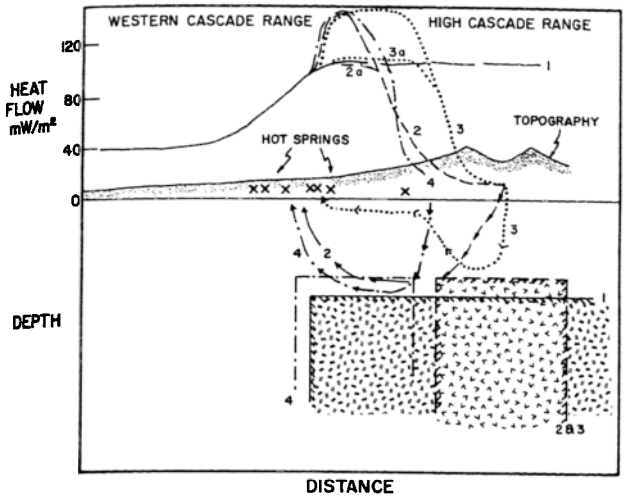

Fig. 7. Several models of the relationship of hot springs to possible heat source positions and the heat flow transition observed near the Western Cascade-High Cascade Range boundary [*Blackwell et al.*, 1978, 1982*a*].

flow presented by *Blackwell et al.* [1982*a*, Figure 10] [see also *Blackwell et al.*, 1978] shown in Figure 7 illustrate various combinations of conductive and convective heat flow and of heat source distributions that might occur in the area. Based on the new data described in the previous sections we can be more specific about the flow conditions for specific areas. The Breitenbush system is apparently similar to flow path 3 in Figure 7 in that part of the flow is stratigraphically controlled. In the Santiam Pass-Belknap/Foley area the flow paths may be more similar to path 2 in Figure 7. In both areas the paths of fluid flow are restricted, and structure is an important control on the location of hot springs and subsurface fluid flow. Only one hole along the west side of the High Cascade Range deeper than 300 m can be used to infer areally distributed fluid flow away from major structures.

Correlation of Volcanism and Curie Point Depths With Regional Thermal Data

In some situations and based on certain assumptions the spacial frequency content of magnetic data can be used to obtain information on the maximum depth of magnetic sources in the crust [*Connard et al.*, 1983]. If this depth is assumed to be controlled by temperature, then an estimate of the depth to the Curie point and some information on crustal temperatures can be obtained. The spatial resolution of the magnetic data is limited because large areas must be averaged to resolve wavelengths from magnetic contrasts at midcrustal depths. *Connard et al.* [1983] used grids about 50 km square to resolve depths to 12 km. Furthermore, there may not be magnetic contrasts at all depths in all areas, with resulting unpredictable results in some regions.

The apparent Curie point depths based on interpretation of the aeromagnetic data [*Connard et al.*, 1983; *Foote*, 1985] are in remarkable agreement with the heat flow data. Areas of shallow Curie point (4–9 km (R. W. Couch, personal communication, 1987)) are compared in Figure 8 to the 50 and 100 mW m^{-2} heat flow contour lines from Figure 1. Outside the enclosed areas calculated depths to the Curie point are in excess of 11 km. *Connard et al.* [1983] and *Foote* [1985] outline the close coincidence between areas of shallow Curie point and high heat flow in the Cascade Range. The average shallow temperature gradient in the high heat flow zone is 65°C km^{-1}. Thus, assuming conductive heat transfer, at depths of 4–9 km predicted temperatures range from 200° to 600°C, depending on the thermal conductivity structure and local variations in heat flow. These temperatures are consistent with Curie temperatures of 300°–580°C for the minerals in typical volcanic rocks [*Connard et al.*, 1983].

The High Cascade Range represents the active volcanic arc associated with subduction of the Juan de Fuca plate and has been the focus of volcanism for the last 5 m.y. [*Taylor*, 1968, this issue; *Priest*, this issue; *Sherrod and Pickthorn*, 1989]. The location of the intrusive centers that can be identified are shown in detail by *Guffanti and Weaver* [1988].

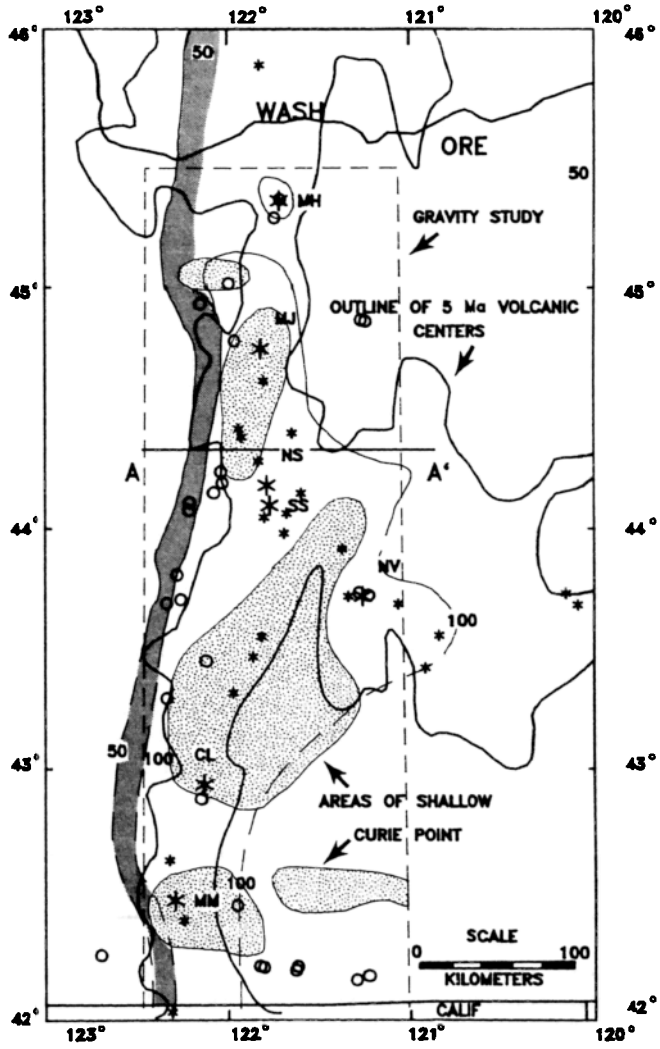

Fig. 8. Comparison of heat flow, outline of 5 Ma volcanic centers [*Guffanti and Weaver*, 1988], and shallow Curie point areas [*Foote*, 1985; R. W. Couch, personal communication, 1987] in the Cascades. The 50 and 100 mW m^{-2} heat flow contours, Holocene volcanoes, and major hot springs (circles) are shown for reference. Area of gravity analysis (the aeromagnetic survey had the same boundaries) and location of section AA′ (Figure 11) are indicated. The area of high lateral heat flow gradient west of the High Cascade Range is shown by the shaded pattern.

The line bounding these centers (from their Figure 4) is shown on Figure 8 for the age range 0–5 Ma. The heat flow gradient lies slightly to the west of the west edge of the line enclosing the centers. However, the arc has been migrating eastward during the last 15 m.y. [see *Blackwell et al.*, 1982*a*; *Verplanck and Duncan*, 1987; *Priest*, this issue], and furthermore the heat flow anomaly at the surface is somewhat wider than the actual heat source [see *Blackwell et al.*, 1982*a*, Figure 8]. Because the thermal processes are averaging over a depth range of 8–20 km and several million years, the colocation of the heat flow and volcanic centers is quite close.

GRAVITY INTERPRETATION

Blackwell et al. [1982*a*] presented an interpretation of the gravity field in the Cascade Range along a cross section at 44°15'N and discussed features that correlate with the heat flow anomaly. *Couch* [1979] and *Couch et al.* [1982*a*, *b*] have published extensive gravity measurements that are suitable for detailed three-dimensional analysis. Thus an areal analysis of the gravity field was carried out as part of this study. The area for which closely spaced gravity data are available is located between 121°W and 122°30'W, longitude, and between 42° and 45°30'N latitude (the area is outlined in Figure 8). This area contains portions of several physiographic provinces including the Western Cascade Range, the High Cascade Range, and small parts of the High Lava Plains, the Basin and Range, and the Deschutes-Umatilla Plateau.

Leaver et al. [1984] analyzed seismic refraction data along a north-south line extending from Mount Hood to Crater Lake. The crustal model interpreted from these data is island arc in character (40 km thick with high average velocity) and shows surprisingly little structural variation along the entire length of the survey. On the other hand, just east of the Cascade Range at Newberry volcano, *Catchings and Mooney* [1988] found that the crust is more Basin and Range in character (i.e., 35 km thick with about equal thicknesses of ≤ 6.2 and ≥ 6.5 km s^{-1} velocities). Thus major crustal variations that might affect the gravity field are east-west (see summary map of crustal thickness of *Mooney and Weaver* [1989]).

Usually, in the analysis of gravity data either the large-scale long-wavelength features (regional) or the small-scale short-wavelength features (residual) are of interest. In either case, it is necessary to determine the regional trends in the data for analysis or removal, depending upon the features of interest. Many different methods have been used to estimate regional trends including low-order polynomial surface fitting and various filtering methods in the frequency domain. The techniques in use have recently been discussed by *Simpson et al.*, [1986]. The regional-residual separation favored by *Simpson et al.* [1986] uses the isostatic "correction" to generate an isostatic residual gravity anomaly from the complete Bouguer gravity anomaly. The isostatic "correction" is calculated assuming perfect Airy-Heiskanen isostasy (a linear correlation of topography to crustal thickness and constant crust/mantle density contrast). The disadvantages of this approach as applied to the region of this discussion are that in this volcanic arc–outer arc setting lateral changes in elastic thickness of the lithosphere and lateral density differences within the crust and mantle due to temperature contrasts must be involved in the isostatic compensation process so the basic assumptions of the "correction" are violated. On a very large scale these deviations may or may not be a problem, but on the scale of the area of this study the effects of the departures from the assumptions of the isostatic "correction" are unknown. Hence the anomaly map resulting from the isostatic regional residual separation may or may not result in an improvement in the understanding of the Cascade gravity field over other techniques of regional residual separation. Moreover, *Simpson et al.* [1986] note that the results of their separation technique often are not too dissimilar to other techniques such as the residual Bouguer correction method [*Aiken and Ander*, 1981], a statistical method relating the gravity field to topography. *Murphey* [1982] used a method similar to the *Aiken and Ander* [1981] technique to analyze the gravity field of the Cascade Range area and reached conclusions identical to those reached below. However, because of the many unknown variables affecting the regional residual separation in the Cascade Range area we will confine our analysis in this discussion to simple wavelength filtering. The conclusions are nonetheless similar to those reached using the isostatic residual gravity anomaly [*Blakely and Jachens*, this issue].

Blakely et al. [1985] and *Blakely and Jachens* [this issue] discussed the gravity field in the Cascade Range and vicinity on the isostatic residual gravity calculated as described by *Simpson et al.* [1986] and upward continued 10 km. *Blakely and Jachens* [this issue] briefly mention two features that will be the focus of this discussion. First, their highly smoothed map shows a 10- to 15-mGal negative anomaly over the Cascade Range in Oregon, and second they locate a north-south boundary between two regions of contrasting crustal density from the latitude of Crater Lake to the latitude of Portland that is 10–20 km west of the west edge of the young volcanic vents (see Figure 8) approximately in the area of the heat flow transition. They note that its location is within 5 km of the gravity gradient described by *Blackwell et al.* [1982*a*]. They do not favor the hypothesis that the boundary is associated with the heat flow anomaly and attribute it instead to a possible geologic contact along a fault. However, as shown by the comparison to the heat flow in Figure 9*a*, the gravity gradient (and the heat flow gradient) is west of the major faults along the west edge of the Cascade Range graben.

Data reduction. A tape of gravity stations with data that included location, observed gravity, free-air and simple Bouguer anomalies, and terrain corrections was the starting point in the analyses [*Couch et al.*, 1982*a*, *b*]. The data on the tape included complete Bouguer anomaly values calculated with an assumed crustal density of 2.67 g cm^{-3}. Although this reduction density may not be strictly valid, the features to be discussed have been shown to exist for reduction densities of 2.43 and 2.28 g cm^{-3} as well [*Blakely et al.*, 1985]. The original data locations are shown by *Couch et al.* [1982*a*, *b*]. For use in the analysis here the gravity data were interpolated to an evenly spaced grid (30 by 98 points) and contoured yielding the complete Bouguer gravity map shown in Figure 9*a*. Digital topographic data were reduced to the same grid as the gravity data. A band-pass topographic map using wavelengths greater than 89.25 km is shown in Figure 9*b* for comparison to the gravity maps. The same wavelength filtering is used to define the regional trends in the gravity data.

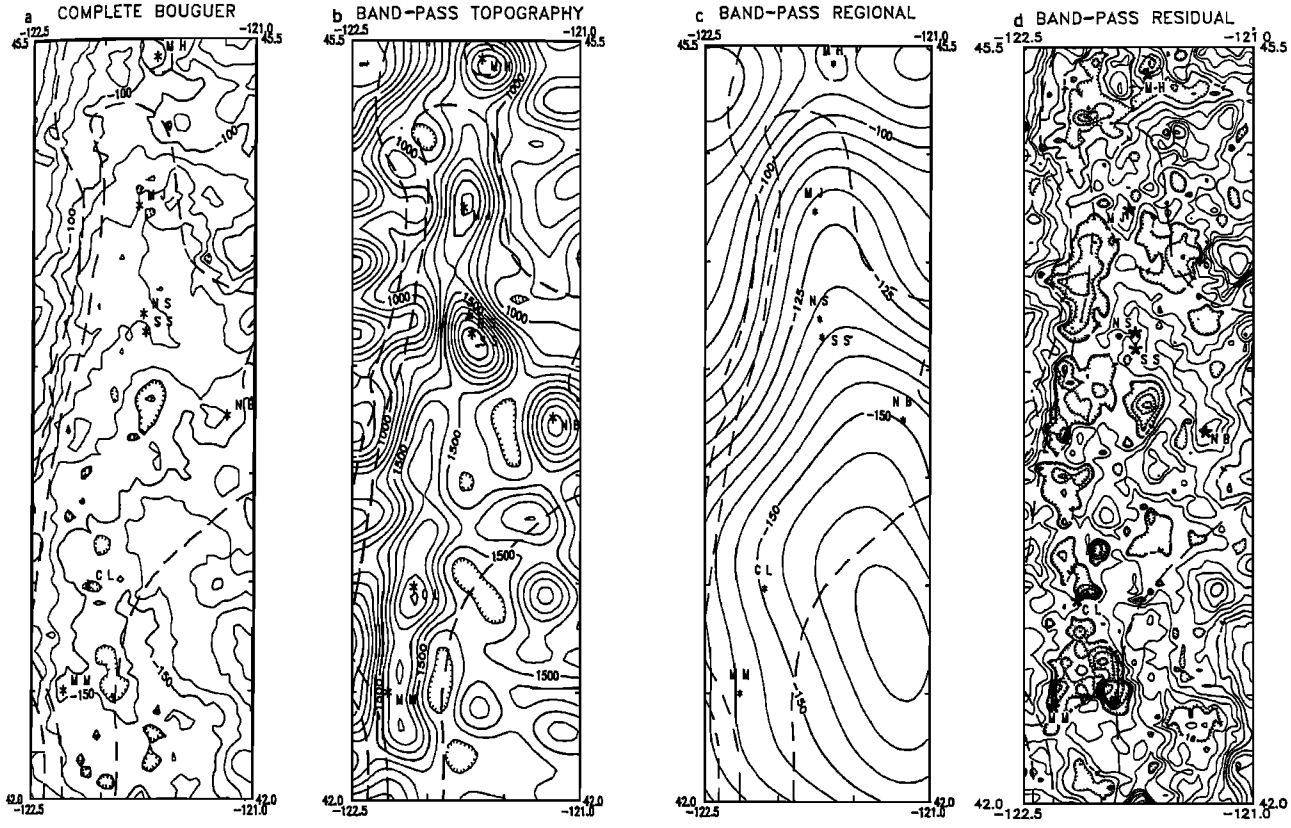

Fig. 9. (*a*) Complete Bouguer anomaly map of the area 121°–122°30'W, 42°–45°30'N. Contour interval is 10 mGal. In these maps and those in Figure 10 the asterisks are, from north to south, Mount Hood, Mount Jefferson, the Sisters, Newberry volcano, Crater Lake, and Mount McLoughlin. In Figures 9 and 10 the 50 and 100 mW m^{-2} heat flow contours from Figure 1*a* are superimposed as dashed lines. (*b*) Regional topography (89.25 km band pass). Contour interval is 100 m. (*c*) Wavelength-filtered regional Bouguer gravity anomaly (89.25 km band pass). Contour interval 5 mGal. (*d*) Residual gravity anomaly map (Figures 9*a* minus Figure 9*c*). Contour interval is 5 mGal.

Discussion of cascade range gravity patterns. Visual analysis of Figure 9*a* reveals a generally west to east decrease in complete Bouguer gravity of more than 50 mGal with the lowest gravity values generally along the axis of the High Cascade Range. The most rapid decrease in Bouguer gravity occurs 10–15 km west of the Western Cascade Range–High Cascade Range boundary and is geographically coincident with the steep heat flow gradient (the 50 and 100 mW m^{-2} contours from Figure 1 are shown on Figures 9 and 10).

The regional gravity, as determined by those features of wavelength >89.25 km, is given in Figure 9*c*. This cutoff wavelength is used by *Couch* [1979] [*Couch et al.*, 1982*b*] to define the regional trends. The value of 89.25 km was determined by inspecting maps of the regional trends created using different cutoff wavelengths and choosing the most representative value. The regional map shows a south plunging trough of low gravity centered over the High Cascade Range. Thus the regional gravity field has a prominent north-south nose in the north half of the map. The "nose" is continuous with the region of most negative values in the southwest Cascade Range and the west edge of the Basin and Range province in the south half of the map. In the southern part of the map the regional gravity may thus be contaminated by Basin and Range trends.

Removal of the regional trends from the observed field (Figure 9*a* minus Figure 9*c*) defines the residual map (Figure 9*d*). The detailed features, with one exception, will not be discussed in this paper as they have been examined by *Couch* [1982*a*, *b*]. The exception is the generally north-south trend of negative anomalies along the west side of the map that is shaded for emphasis. This anomaly is discussed below.

Motivation for heat flow model. A prominent feature in the residual map (Figure 9*d*) is the linear negative residual anomaly along the western edge of the study area. Comparison of the trend of the anomalies to the heat flow contours shows that west edge of the residual low directly coincides with the heat flow gradient. The west edge also coincides with the boundary identified by *Blakely and Jachens* [this issue]. Because of the close correlation of the gravity and heat-flow gradients and the lack of major changes in rock composition or density, *Blackwell et al.* [1982*a*] argued that the mechanism responsible for the rapid change in gravity may be related to the one responsible for the change in heat flow.

There are also coincidental features between the heat flow and regional gravity anomaly pattern (Figure 9*c*). The axis of the south plunging trough in the regional gravity field coincides with the volcanic axis and the area of high heat flow. In order to determine if the heat flow and gravity data could be related, a three-dimensional density difference model was calculated using the heat flow data, and its effects on the gravity fields shown in Figures 9*b* and 9*c* were examined.

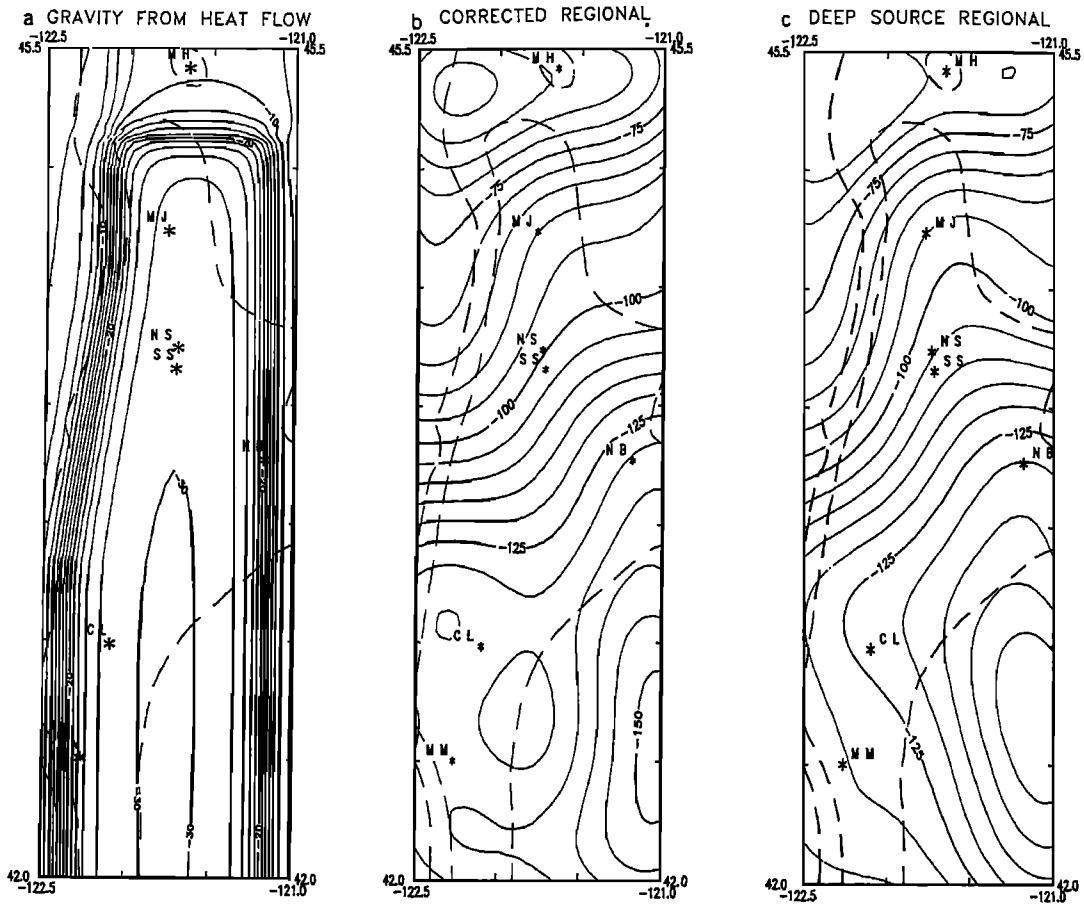

Fig. 10. (*a*) Gravity anomaly predicted from heat flow [*Blackwell et al.*, 1982*a*, model B]. Contour interval is 2 mGal. (*b*) Band-passed regional gravity corrected for crustal heat source effect (model B). Contour interval is 5 mGal. (*c*) Band-passed regional gravity corrected for thermal effect at the crust/mantle boundary. Contour interval is 5 mGal.

Blackwell et al. [1982*a*] derived a density difference versus depth structure for the volcanic arc versus the outer arc block by first subtracting characteristic outer arc crustal temperatures from the calculated temperatures under the High Cascade Range and then multiplying the temperature differences by a coefficient of thermal expansion. The outer arc temperatures were calculated using average surface gradients and heat flow, known thermal conductivities, and presumed radioactivity distributions. The volcanic arc temperatures came from the downward continued heat flow data (calculated using the method of *Brott et al.* [1981]). This procedure was used to generate density difference model A [*Blackwell et al.*, 1982*a*, Figure 9]. Such a density difference model generates a gravity effect of only 10 mGal in contrast to the 25 mGal observed (although note that the anomaly isolated by *Blakely and Jachens* [this issue] has an amplitude of about 15 mGal). In order to obtain a 25-mGal gravity anomaly and to fit the gradient, the density contrast between 6 and 10 km was raised from 0.035 to 0.15 g cm^{-3} (model B [*Blackwell et al.*, 1982*a*, Figure 9]). A density contrast of this magnitude cannot be explained by thermal expansion alone, so a phase change such as regions of partial melting, or a change in composition is needed to account for the contrast. Actual density changes associated with melting are not known in detail. *Oppenheimer and Herkenhoff* [1981] found that a density contrast of -0.4 to -0.5 g cm^{-3} was needed to model gravity data over The Geysers area in California, and *Eaton et al.* [1975] used a density contrast of -0.22 g cm^{-3} for igneous rocks beneath the Yellowstone caldera. So the density contrast of -0.15 g cm^{-3} assumed by *Blackwell et al.* [1982*a*] might be generated by an area with a small (but unknown) amount of melt, by a compositional contrast, or by some combination of the two effects.

Based on the assumption that temperature and heat flow are related to density contrasts, the two-dimensional density differences were extended into three dimensions as rectangular prisms of finite length. Model B was used to represent the high-temperature region under the High Cascade Range. Where thermal data are sparse, the regions of shallow Curie point identified from aeromagnetic data [*Connard et al.*, 1983; *Foote*, 1985] were used to constrain the prism boundaries. The resulting calculated gravity model was not adjusted to better "fit" the data.

The gravity field of the thermal model calculated using a three-dimensional Talwani approach [*Talwani and Ewing*, 1960] is illustrated in Figure 10*a*. In order to determine to what extent the thermal structure affects the gravity, the calculated gravity was subtracted from the original complete Bouguer anomaly values (Figure 9*a*). The "heat flow corrected" data were then transformed, and a new band-pass regional (with 89.25 km cutoff wavelength) calculated. The "heat flow corrected" regional anomaly map is shown in Figure 10*b*.

Discussion of "heat flow corrected" regional gravi-

ty. The difference between the "heat flow corrected" regional gravity (Figure 10*b*) and the noncorrected regional trends (Figures 9*c*) is interesting. In the "heat flow corrected" regional gravity (Figure 10*b*), almost all traces of the south plunging trough present in the original data in the north half of the map have been removed. As shown in Figure 10*b*, the orientation of the contours across the north half of the study area is northeast-southwest.

Outside the map area, to the northeast, there is a similar northeast-southwest trend with a regional gravity contrast of about 50 mGal [*Riddihough et al.*, 1986]. This gradient is associated with fundamental crustal and/or upper mantle differences between the Columbia Plateau and the Blue Mountains/Basin and Range provinces. This northeast-southwest regional gradient is obscured in the area of the Cascade Range (Figure 9*c*) due to the negative anomaly associated with the area. On the other hand, the north half of the regional map after the "heat flow correction" is applied (Figure 10*b*) is dominated by a northeast-southwest gradient that directly connects to the Blue Mountains/Basin and Range transition.

Gravity effect of Cascade Range "graben." In examining the gravity data for the Cascade Range, *Couch et al.* [1982*a*, *b*] and *Blakely et al.* [1985] interpreted the narrow north-south trending negative anomaly shown in Figure 9*d* as the signature of the proposed Cascade graben of *Allen* [1965]. This anomaly is west of most major stratovolcanoes (Mount Hood, Mount Jefferson, Three Sisters, Crater Lake), although it swings southwest to include Mount McLoughlin. *Couch et al.* [1982*a*, *b*] proposed a displacement along the west side of the graben of the order of 1.2–1.5 km. The high surface heat flow was not considered as an influence on the gravity data.

A problem with this model is that the original gravity map (Figure 9*a*) has no north-south high-frequency gradient that could correspond to the east edge of the graben. Because of the shallow and abrupt nature of any such boundary, it cannot be isostatically compensated and, if present, should be obvious. A second problem is that the location of the negative anomaly is west of the High Cascade Range and, as noted by *Blakely and Jachens* [this issue], does not coincide with the surface exposures of the normal faults. Thus *Blackwell et al.* [1982*a*] argued that the gradient along the west side of the map was related to density changes in the midcrust associated with the edge of the high-temperature zone. The east edge of the high heat flow region is not obvious because the crust is also thermally disturbed in the Basin and Range province. An alternative explanation is that the wave length filtering approach is inappropriate in this case, as was suggested by *Murphey* [1982].

The conclusions of this section are not taken to indicate that there is not an axial graben, only that there does not appear to be much density contrast associated with any graben fill. In fact, if the graben is asymmetric, as the reflection data imply for the Santiam Pass area [*Keach et al.*, 1989], part of the gravity gradient could be due to the graben fill (although the location mismatch prevents the graben model from explaining most of the anomaly).

Crust-mantle model. In order to help in understanding the limits of models that can satisfy the two features of the Cascade Range gravity field that have been discussed, a third, deep-source model was examined. A deeply buried zone of density contrast (at 40 km, corresponding to the crust-mantle boundary) having the same shape as the heat flow model previously discussed was used. The gravity effect due to this source was calculated and removed from the complete Bouguer gravity field and the band-pass regional recalculated (Figure 10*c*). Since the signal due to the deep source is broad, its effect is seen over the whole map area, so the shape of the regional anomaly shown in Figure 9*c* is not substantially changed, and thus the NE-SW Blue Mountain trend is not accentuated. Also any high-frequency features such as those shown in Figure 9*d* would not be affected by this deep-seated low-density mass.

Conclusions of gravity analysis. The results of the study illustrate the basic relationships of the thermal field and gravity fields. Two features that can be explained by this relationship have been described. First, the removal of the "heat flow related effects" on the gravity field results in outside trends in the gravity being projected through the study area. Second, this removal also suppresses the linear trend of negative residual anomalies along the west side of the study area that correlates directly with the heat flow transition. The density contrasts that cause these features must be in the mid to upper crust. The close correlation between regional gravity and heat flow may be evidence of one source mechanism for both data sets. Alternatively, part of the relationship could be indirect in that compositional changes in the midcrust (the boundary of the 6.5 km s^{-1} layer identified by *Leaver et al.* [1984]) and/or density changes in some shallow layers that are related to High Cascade Range structure could explain the gravity data. The alternative models present different valid ways of explaining the observed gravity field; however, based on this discussion, we do not believe that interpretation of Cascade Range gravity data can neglect thermal effects.

DISCUSSION

Geophysical characteristics of the midcrust. It is argued in this paper that the regional thermal, gravity and magnetic data point toward a major, long-lived, heat source and the consequent existence of high temperatures in the midcrust beneath the High Cascade Range in northern Oregon. This heat source extends about 30 km on average west of the Quaternary volcanic axis and is broader than the zone of Quaternary volcanism and deformation. It appears to have existed for at least several millions of years, if not for the life of the volcanic arc. Some of the data are summarized in map form on Figure 8, and in this section the results are illustrated in cross-section form in Figure 11.

In earlier discussions of heat flow data, *Blackwell et al.* [1978, 1982*a*] (see Figure 7) outlined the possible groundwater circulation patterns which might generate the heat flow patterns and geothermal systems observed in the Western Cascade Range/High Cascade Ranges. Recently, *Ingebritsen et al.* [1989] have proposed that all the high heat flow along the Western Cascade Range/High Cascade Range boundary is related to groundwater circulation and not to a midcrustal heat source. They suggest that the heat flow is about 60 mW m^{-2} along the High Cascade/Western Cascade Range boundary and that the heat source is confined more narrowly to the axis of the High Cascade Range. We proposed this model as an alternative to the our preferred interpretation over 10 years ago. In fact, their model is exactly represented by fluid flow curves 2a/3a and source region 2/3 on Figure 7 (taken from *Blackwell et al.* [1978]).

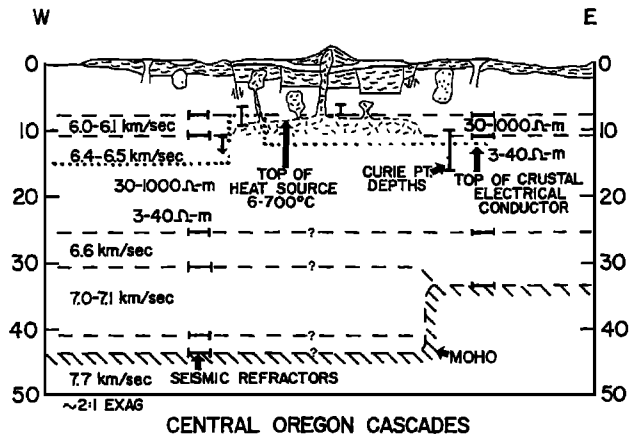

Fig. 11. Generalized cross section of the northern Oregon Cascade Range summarizing geophysical results. Dotted line is the upper boundary of the crustal low-resistivity region. Vertical bars show locations of Curie point depth determinations. Horizontal bars are positions of crustal boundaries determined by seismic refraction lines.

We believe the evidence and favors the model discussed here and by *Blackwell et al.* [1982*a*] as a regional explanation and that the narrower heat source is not consistent with the geophysical data discussed above and summarized below. As shown in Figure 8, when the heat flow anomaly is compared to the areas of volcanic sources over the past 5 m.y. as described by *Guffanti and Weaver* [1988], there is a closer correlation between the width of the source zone and the width of the intrusive centers. As noted by *Blackwell et al.* [1982*a*] and described in detail by *Priest* [this issue] the axis of the volcanic arc is migrating eastward with time, so an asymmetric thermal anomaly might be expected. Since the thermal process over a depth and/or distance range of 10 km average over several million years, the coincidence of the data sets is consistent with the interpretation of a mid to upper crust, regional scale, heat source.

Since our first discussion [*Blackwell et al.*, 1978, 1982*a*], heat flow studies in British Columbia [*Lewis et al.*, 1988] and Washington [*Blackwell et al.*, this issue] have outlined similar anomalies in those parts of the Cascade Range. In particular the 10 km half width of the west edge of the high heat flow anomaly is a characteristic feature. The geologic setting of these areas is quite different, and hydrology can hardly be the cause of the similar half widths in all three areas.

Ingebritsen et al. [1989] argue on the basis of energy loss that all the background heat is swept from the High Cascade Range to the hot springs and that the heat flow is 0 mW m^{-2} in the High Cascade Range. They base their conclusions on a heat flow in the High Cascade Range of 100 mW m^{-2}(?). However, near the axis, and near the major volcanic centers, the heat loss is much higher than 100 mW m^{-2} (i.e., the example of Mount Hood discussed by *Steele et al.* [1982]). Therefore the heat loss in the hot springs does not a priori furnish information to constrain the nature of fluid flow in the systems. They also apparently envision near-zero heat flow to great depth beneath the High Cascade Range because of the sweeping of the heat at temperatures of at least 100°C to the hot springs along the west side.

In contrast, we postulate only a shallow low heat flow zone so that the majority of the groundwater is heated only a few degrees at most. We believe that the evidence suggests that the bulk of the volcanic rocks below a few hundred meters in depth have been subjected to alteration at moderate temperatures during deposition and burial. In the absence of tectonic activity to form and to keep open fractures (at the present time, as noted above, the Cascade Range in Oregon is essentially aseismic), these rocks are relatively impermeable. The permeability may increase deeper in the crust where the rocks have been subjected to alteration at 250°C or so (at these temperatures the rocks will be more brittle and capable of sustaining open fractures). Only along major structures and particularly favorable horizons is flow to depths of over 1 km likely to affect the heat transfer. Consequently, only a fraction of the background heat flow is released at the concentrated thermal anomalies at the hot springs and in hot fluid flow. The agreement between the depth to Curie point and heat flow data is also inconsistent with temperatures at several kilometers that are significantly below those predicted on the basis of conductive heat transfer and is an additional argument against major regional water flow effects on regional temperatures in the crust.

The apparent Curie point depths discussed by *Connard et al.* [1983] based on interpretation of aeromagnetic data are in close agreement with the heat flow data given the limited spacial resolving power of the analysis technique. Areas of shallow Curie point based on a spectral analyses of the magnetic data were shown in Figure 8. These results are shown diagrammatically in Figure 11 as vertical bars giving the variation of depth to the Curie point over a particular cross section of the High Cascade Range at 44°15′ latitude near the intersection with the High Lava Plains (AA′ in Figure 8).

Stanley et al. [this issue] have described extensive magnetotelluric measurements of crustal resistivity in western Oregon and Washington. There is no one-to-one match of the heat flow and resistivity data. In places there is quite close coincidence, whereas in others the agreement is not so good. For example, the results from the profile across central Oregon are shown as the dotted line, which represents the boundary between areas of resistivity of 30–1000 Ω m above and 3–40 Ω m below (Figure 11). Clearly, temperature alone is not sufficient to explain the resistivity distribution, and *Stanley et al.* [this issue] invoke fluids and mineralogic variations as well to explain the resistivity distribution. Most pertinent are several profiles in central Oregon between 44° and 45°15′N that cross the heat flow transition [*Stanley et al.*, this issue, Figure 5]. The three profiles illustrated all show an upwarp of the deep crustal conductor at the edge of the heat flow transition, not the edge of the volcanic centers. Typical depths to the top of the conductor beneath the Cascade Range are 10–18 km, and all three profiles show depths of 6–8 km at the transition. However, *Stanley et al.* [this issue] note that the resolution of the MT models along the axis of the High Cascade Range is poor and favor a model with a shallower top to the low-resistivity layer than the MT modeling predicts so that the low-resistivity zone will correspond to the depth of the 6.5 km s^{-1} layer.

Additional regional resistivity measurements have been made by the EMSLAB group [*EMSLAB Group*, 1988; *Booker and Chave*, 1989; *Livelybrooks et al.*, 1989]. Their results in the Cascade Range are similar the those of *Stanley*

et al. [this issue]. They found a similar region of low resistivity in the midcrust and outlined a region of very low resistivity below the Western-High Cascade Range boundary between depths of 5 and 15 km. Similarly, *Hermance et al.* [1989] found a deep crustal conductor contiguous with one in the Basin and Range and extending westward into the edge of the Western Cascade Range. *Hermance et al.* [1989] also located the top of the conductor at about 15 km.

Stanley et al. [this issue] consider the low resistivity zone to be coincident with the 6.5 km s^{-1} layer and to be caused by "metamorphically produced fluids and partial melt." Their postulated thermal conditions needed to satisfy the MT results are 600°C at 15 km, not inconsistent with a "zone of intense thermal disturbance, at a depth of the order of 10 ± 2 km and a temperature as high as 700 ± 100°C" postulated by *Blackwell et al.* [1982*a*, p. 8750].

Figure 11 shows a summary cross section from the results of seismic, thermal, magnetic, and electric investigations. The refraction results of *Leaver et al.* [1984] and *Catchings and Mooney* [1988] discussed above are represented by the horizontal groups of bars on the east and west sides of the section. No data are available for the area between Newberry volcano and the Western Cascade Range except along the line of a reflection profile that does not furnish information on deep crustal structure [*Keach et al.*, 1989]. In the Western Cascade Range the crust is over 40 km thick, whereas in the High Lava Plains it is approximately 35 km thick. The High Lava Plains have a velocity structure and crustal thickness more typical of the Basin and Range province because the crust is composed of approximately equal portions with seismic velocity below and above 6.5 km s^{-1}. On the other hand, the Western Cascade Range crust has a velocity distribution more typical of an island arc because velocities below 6.5 km s^{-1} make up only 25% of the total crustal thickness. Unfortunately, the data do not allow resolution of where the change in crustal type occurs across the High Cascade Range.

One argument against a significant amount of partial melt in the midcrust is that a low-velocity layer is not required by the seismic refraction interpretation [*Leaver et al.*, 1984]. However, the profile line was along the edge of the heat source, so that faster paths along the outer arc block would be preferred. Also isolated zones of partial melt might not be detailed in any event.

Blackwell et al. [1982*a*] interpreted the heat source to represent a major staging magma chamber or zone of magma residence underlying most of the High Cascade Range and at a temperature near the melting for silicic rocks. Upper crustal rocks that are in contact with the heat source could be at least partially melted at either isolated or contiguous locations. Physical conditions at this depth would be pressures on the order of 3 kbar and temperatures of the order 600°–800°C. Interpretation of the results from the southern Washington Cascade Range suggest a similar depth to the heat source but indicate a temperature of only 400°–500°C at equivalent depths [*Blackwell et al.*, this issue]. There should be no partial melt available on a regional basis in Washington, although small pockets are not resolvable as individual bodies because of the sparse heat flow data.

In the case of the crust beneath Oregon it is enticing to think that the apparent location of the heat source is related to the transition indicated by the seismic refraction data from higher densities associated with velocities of 6.4–6.5 km s^{-1} to lower densities associated with upper crustal velocities of 6.0–6.1 km s^{-1} at a depth of about 10 km. The significant density change might localize intrusion if the magmas do not have significant hydraulic head to reach the surface [*Ryan*, 1987]. However, in the Washington Cascade Range, such an interpretation is not as viable because the upper crust is more silicic and the major crustal density change occurs well below the depth to the top of the heat source. Therefore, in the case of the Washington Cascade Range at least, the major factor may be the rapid decrease in temperature above depths of 10 km associated with the bottom of the upper crustal radioactive layer. Some unknown structural discontinuity might also provide the localizing effect.

The interpretation of the heat source area as a magma staging region is discussed in more detail by *Blackwell et al.* [this issue], a companion paper, so the comments here are relevant primarily to the Oregon Cascade Range. Average temperatures in the midcrust are extremely high, as high as 700°–800°C at 8–12 km. The composition of material intruded into the magma staging region is not resolved at the present time but is certainly complex and time varying. *Sherrod* [1986] reached a tentative conclusion based on phase equilibria that the basaltic and basaltic andesite magmas in the central High Cascade Range in Oregon equilibrated at 10–15 km before their eruption. Also not known is whether there might a more or less continuous zone of gabbroic intrusives underlying the heat source (perhaps making up the upper part of the 6.5 km s^{-1} layer) or whether pockets of gabbroic magma in the lower crust or at the crust/mantle contact [*Hildreth and Moorbath*, 1988] generate the secondary magmas there by partial melting and by fractional crystallization which subsequently move up and form part of the midcrustal heat source identified by the heat flow data. The geographic coincidence of a number of geophysical features may be due directly or indirectly to nonthermal causes, but we prefer to see them as related. Further detailed studies of this area should shed much light on the geological and geophysical features associated with crustal magmatism and metamorphism.

Acknowledgments. Most of the studies described in this paper have been supported by USDOE. Collection and interpretation of the Cascade Range thermal data in particular has been supported by USDOE grant DG-FG07-86ID12623 to SMU. Edward Western and John Knox were responsible for permission to use extensive SUNEDCO exploration results in the Breitenbush and Santiam Pass areas; Kichurl Lee calculated terrain corrections and heat flow values for the Santiam Pass data. Richard Couch made available a tape of the original gravity data for the area of the gravity analysis. Colin Williams and L. J. P. Muffler reviewed this manuscript and made many valuable comments.

REFERENCES

Aiken, C. L. V., and M. E. Ander, A regional strategy for geothermal exploration with emphasis on gravity and magnetotellurics, *J. Volcanol. Geotherm. Res.*, *9*, 1–27, 1981.

Allen, J. E., The Cascades Range volcano-tectonic depression of Oregon, in *Transactions of the Lunar Geological Field Conference, Bend, Oregon, August, 1965*, pp. 21–23, Oregon Department of Geological and Mineral Industries, Portland, 1965.

Atwater, B. F., Evidence for great Holocene earthquakes along the outer coast of Washington State, *Science*, *236*, 942–944, 1987.

Barger, K. E., Secondary mineralogy of core from geothermal drill hole CTGH-1, Cascade Range, Oregon, Geology and Geothermal Resources of the Breitenbush-Austin Hot Spring Area, Clackmas

and Marion Counties, Oregon, edited by D. R. Sherrod, *Open File Rep. 0-88-5*, pp. 39–48, Portland, 1988.

Beall, J., A hydrologic model based on deep test data from the Walker "O" No. 1 well, Terminal Geyser, California, *Trans. Geotherm. Resour. Counc.*, *5*, 153–156, 1981.

Black, G. L., D. D. Blackwell, and J. L. Steele, Heat flow in the Oregon Cascades, *Geology and geothermal resources of the central Oregon Cascade Range*, edited by G. R. Priest and B. F. Vogt, *Spec. Pap. Oreg. Dep. Geol. Miner. Ind.*, *15*, 69–76, 1983*a*.

Black, G. L., M. Elliott, J. D'Alluva, and B. Purdom, Results of a geothermal resource assessment of the Ashland, Oregon, area, Jackson County, *Oreg. Geol.*, *45*, 51–55, 1983*b*.

Black, G. L., G. R. Priest, and N. M. Woller, Temperature data and drilling history of the Sandia National Laboratories well at Newberry caldera, *Oreg. Geol.*, *46*, 7–9, 1984.

Black, G. L., N. M. Woller, and M. L. Ferns, Geologic map of the Crescent Mountain area, Linn County, Oregon, *Geol. Map Ser. 47*, Oreg. Dep. of Geol. Miner. Ind., Portland, 1987.

Blackwell, D. D., Thermal structure of the continental crust, pp. 169–184, *The Structure and Physical Properties of the Earth's Crust*, *Geophys. Monogr. Ser.*, vol. 14, edited by J. G. Heacock, pp. 169–184, AGU, Washington, D. C., 1971.

Blackwell, D. D., Heat flow and energy loss in the Western United States, Cenozoic Tectonics and Regional Geophysics of the Western Cordillera, edited by R. B. Smith and G. P. Eaton, pp. 175–208, *Mem. Geol. Soc. Am.*, *152*, 175–208, 1978.

Blackwell, D. D., A transient model of the geothermal system of the Long Valley caldera, California, *J. Geophys. Res.*, *90*, 11,229–11,241, 1985.

Blackwell, D. D., and S. L. Baker, Thermal analysis of the Breitenbush geothermal system, *Trans. Geotherm. Resour. Counc.*, *12*, 221–227, 1988*a*.

Blackwell, D. D., and S. L. Baker, Thermal analysis of the Austin and Breitenbush geothermal systems, Western Cascades, Geology and Geothermal Resources of the Breitenbush-Austin Hot Spring Area, Clackmas and Marion Counties, Oregon, edited by D. R. Sherrod, *Open File Rep. 0-88-5*, pp. 44–62, Oreg. Dep. of Geol. and Miner. Ind., Portland, 1988*b*.

Blackwell, D. D., and R. E. Spafford, Experimental methods in continental heat flow, *Exp. Methods in Phys.*, *24*, 189–226, 1987.

Blackwell, D. D., and J. L. Steele, A summary of heat flow studies in the Cascade Range, *Trans. Geotherm. Resour. Counc.*, *7*, 233–236, 1983*a*.

Blackwell, D. D., and J. L. Steele, Thermal model of the Newberry Volcano, Oregon, Survey of Potential Geothermal Exploration Sites at Newberry Volcano Deschutes County, Oregon, *Open File Rep. 9-83-3*, pp. 83–113, Oreg. Dep. of Geol. and Miner. Ind., Portland, 1983*b*.

Blackwell, D. D., and J. L. Steele, Geothermal data from deep holes in the Oregon Cascade Range, *Trans. Geotherm. Resour. Counc.*, *11*, 317–322, 1987.

Blackwell, D. D., D. A. Hull, R. G. Bowen, and J. L. Steele, Heat flow of Oregon, plus 1:1,000,000 scale map, *Spec. Pap. Oreg. Dep. Geol. Miner. Ind.*, *4*, 42 pp., 1978.

Blackwell, D. D., J. L. Steele, and C. A. Brott, The terrain effect on terrestrial heat flow, *J. Geophys. Res.*, *85*, 4757–4772, 1980.

Blackwell, D. D., R. G. Bowen, D. A. Hull, J. Riccio, and J. L. Steele, Heat flow, arc volcanism, and subduction in northern Oregon, *J. Geophys. Res.*, *87*, 8735–8754, 1982*a*.

Blackwell, D. D., C. F. Murphey, and J. L. Steele, Heat flow and geophysical log analysis for OMF-7A geothermal test well, Mt. Hood, Oregon, *Spec. Pap. State Oreg. Dep. Geol. Miner. Ind.*, *14*, 47–56, 1982*b*.

Blackwell, D. D., J. L. Steele, and S. A. Kelley, Heat flow and geothermal studies in the State of Washington, *U.S. DOE Rep. ID/12307-1*, 77 pp., Department of Energy, Washington, D. C., 1985.

Blackwell, D. D., J. L. Steele, and L. Carter, Heat flow data base for the United States, in *Geophysics of North America CD-ROM*, edited by A. M. Hittleman, J. O. Kinsfather, and H. Meyers, National Oceanic and Atmospheric Administration, National Geophysical Data Center, Boulder, Colo., 1989.

Blackwell, D. D., J. L. Steele, and L. Carter, DNAG Geothermal Map of North America, scale 1:5,000,000, *Geol. Soc. Am.*, in press, 1990.

Blackwell, D. D., J. L. Steele, S. A. Kelley, and M. Korosec, Heat flow in the state of Washington and thermal conditions in the Cascade Range, *J. Geophys. Res.*, this issue.

Blakely, R. J., and R. C. Jachens, Volcanism, isostatic residual gravity, and regional tectonic setting of the Cascade volcanic province, *J. Geophys. Res.*, this issue.

Blakely, R. J., R. C. Jachens, R. W. Simpson, and R. W. Couch, Tectonic setting of the southern Cascade Range as interpreted from its magnetic and gravity fields, *Geol. Soc. Am. Bull.*, *96*, 43–48, 1985.

Booker, J. R., and A. D. Chave, Introduction to the special section on the EMSLAB-Juan de Fuca experiment, *J. Geophys. Res.*, *94*, 14,093–14,098, 1989.

Brook, C. A., R. H. Mariner, D. R. Mabey, J. R. Swanson, M. Guffanti, and L. J. P. Muffler, Hydrothermal convection systems with reservoir temperatures ≥90°C, Assessment of Geothermal Resources of the United States—1978, edited by L. J. P. Muffler, *U.S. Geol. Surv. Circ.*, *790*, 18–85, 1979.

Brott, C. A., D. D. Blackwell, and P. Morgan, Continuation of heat flow data: A method to construct isotherms in geothermal areas, *Geophysics*, *46*, 1732–1744, 1981.

Catchings, R. D., and W. D. Mooney, Crustal structure of east central Oregon: Relation between Newberry volcano and regional crustal structure, *J. Geophys. Res.*, *93*, 10,081–10,094, 1988.

Connard, G., R. W. Couch, and M. Gemperle, Analysis of aeromagnetic measurements from the Cascade Range in central Oregon, *Geophysics*, *48*, 376–390, 1983.

Couch, R. W., Geophysical investigations of the Cascades Range in central Oregon, final report, grant 14-08-001-G-393, 95 pp., U.S. Geol. Surv., Reston, Va., 1979.

Couch, R. W., G. S. Pitts, M. Gemperle, D. E. Braman, and C. A. Veen, Gravity anomalies in the Cascade Range in Oregon: Structural and thermal implications, *Open File Rep. 0-82-9*, 66 pp., Oreg. Dep. of Geol. and Miner. Ind., Portland, 1982*a*.

Couch, R. W., G. S. Pitts, M. Gemperle, C. A. Veen, and D. E. Braman, Residual gravity maps of the northern, central, and southern Cascade Range, Oregon, 121°00′ to 122°30′W by 42°00′ to 45°N, *Geol. Map Ser. GMS-26*, scale 1:250,000, Oreg. Dep. of Geol. and Miner. Ind., Portland, 1982*b*.

Couch, R. W., M. Gemperle, and R. Peterson, Total-field aeromagnetic anomaly maps, Cascade Mountain Range, northern Oregon, *Geol. Map Ser. GMS-40*, scale 1:250,000, Oreg. Dep. of Geol. and Miner. Ind., Portland, 1985.

Eaton, G. P., R. L. Christensen, H. M. Iyer, A. M. Pitt, I. Zietz, and M. E. Gettings, Magma beneath Yellowstone National Park, *Science*, *188*, 787–796, 1975.

EMSLAB Group, The EMSLAB electromagnetic sounding experiment, *Eos Trans. AGU*, *69*, 89–99, 1988.

Foote, R. W., Curie-point isotherm mapping and interpretation from aeromagnetic measurements in the northern Oregon Cascades, M.S. thesis, 115 pp., Oreg. State Univ., Corvallis, 1985.

Guffanti, M., and C. S. Weaver, Distribution of late Cenozoic volcanic vents in the Cascade Range (USA): Volcanic arc segmentation and regional tectonic considerations, *J. Geophys. Res.*, *93*, 6513–6529, 1988.

Heaton, T. H., and S. H. Hartzell, Earthquake hazards of the Cascadia subduction zone, *Science*, *236*, 162–168, 1987.

Hermance, J. F., S. Lusi, W. Slocum, G. A. Neumann, and A. W. Green, Jr., A high-density remote reference magnetic variation profile in the Pacific Northwest of North America, *Phys. Earth. Planet. Inter.*, *53*, 305–319, 1989.

Hildreth, W., and S. Moorbath, Crustal contributions to arc magmatism in the Andes of central Chile, *Contrib. Mineral. Petrol.*, *98*, 455–489, 1988.

Hyndman, R. D., Heat flow measurements in the inlets of southwestern British Columbia, *J. Geophys. Res.*, *81*, 337–349, 1976.

Ingebritsen, S. E., D. R. Sherrod, and R. H. Mariner, Heat flow and hydrothermal circulation in the Cascade Range, north-central Oregon, *Science*, *243*, 1458–1462, 1989.

Keach, R. W., II, J. E. Oliver, L. D. Brown, and S. Kaufman, Cenozoic active margin and shallow Cascades structure: COCORP results from western Oregon, *Geol. Soc. Am. Bull.*, *101*, 783–794, 1989.

Leaver, D. S., W. D. Mooney, and W. M. Kohler, A seismic refraction study of the Oregon Cascades, *J. Geophys. Res.*, *89*, 3121–3134, 1984.

Lewis, T. J., A. H. Jessop, and A. J. Judge, Heat flux measure-

ments in southwestern British Columbia: The thermal consequences of plate tectonics, *Can. J. Earth. Sci.*, *22*, 1261–1273, 1985.

Lewis, T. J., W. H. Bentkowski, E. E. Davis, R. D. Hyndman, J. G. Souther, and J. A. Wright, Subduction of the Juan de Fuca plate: Thermal consequences, *J. Geophys. Res.*, *93*, 15,207–15,225, 1988.

Livelybrooks, D. W., W. W. Clingman, J. T. Rygh, S. A. Urquhart, and H. S. Waff, A magnetotelluric study of the High Cascades graben in central Oregon, *J. Geophys. Res.*, *94*, 14,173–14,184, 1989.

Ludwin, R. S., C. S. Weaver, and R. S. Crosson, Seismicity of Oregon and Washington, in *The Geology of North America*, vol. CSMV-1, *Neotectonics of North America*, edited by D. B. Slemmons, E. R. Engdahl, and D. D. Blackwell, Geological Society of America, Boulder, Colo., in press, 1990.

Mariner, R. H., J. S. Presser, W. C. Evans, and M. K. W. Pringle, Discharge rates of fluids and heat by thermal springs of the Cascade Range, Oregon, Washington and northern California, *J. Geophys. Res.*, this issue.

Mase, C. W., J. H. Sass, A. H. Lachenbruch, and R. J. Munroe, Preliminary heat-flow investigations of the California Cascades, *U.S. Geol. Surv. Open File Rep.*, *82-150*, 240 pp., 1982.

Mooney, W. D., and C. S. Weaver, Regional crustal structure and Tectonics of the Pacific Coastal states: California, Oregon, and Washington, Geophysical Framework of the Continental United States, edited by L. C. Pakiser and W. D. Mooney, *Mem. Geol. Soc. Am.*, *172*, 129–161, 1989.

Murphey, C. F., An investigation of the Cascade Range of Oregon through the use of gravity, topography, and heat flow, M.S. thesis, South. Methodist Univ., Dallas, Tex., 1982

Oppenheimer, D. H., and K. E. Herkenhoff, Velocity-density properties of the lithosphere from three dimensional modeling at The Geysers–Clear Lake area, California, *J. Geophys. Res.*, *86*, 6057–6065, 1981.

Peck, D. L., A. B. Griggs, H. G. Schliker, and H. M. Dole, Geology of the central and northern parts of the Western Cascade Range in Oregon, *U.S. Geol. Surv. Prof. Pap.*, *449*, 56 pp., 1964.

Priest, G. R., Volcanic and tectonic evolution of the Cascade volcanic arc, central Oregon, *J. Geophys. Res.*, this issue.

Priest, G. R., N. M. Woller, and G. L. Black, Overview of the central Oregon Cascade Range, Geology and Geothermal Resources of the central Oregon Cascade Range, edited by G. R. Priest, and B. Vogt, *Spec. Pap. Oreg. State Dep. Geol. Miner. Ind.*, *15*, 3–28, 1983.

Priest, G. R., N. M. Woller, and M. L. Fens, Geologic map of the Breitenbush River area, Linn and Marion counties, *Geol. Map Ser. 46*, scale 1:62,500, Oreg. Dep. of Geol. and Miner. Ind., Portland, 1987.

Priest, G. R., G. L. Black, and N. M. Woller, Geologic map of the McKenzie Bridge Quadrangle, Lane County, Oregon, *Geol. Map Ser. 48*, Oreg. Dep. of Geol. and Miner. Ind., Portland, 1988.

Rasmussen, J., and E. Humphreys, Topographic image of the Juan de Fuca plate beneath Washington and western Oregon using teleseismic *P*-wave travel times, *Geophys. Res. Lett.*, *15*, 1417–1420, 1988.

Riddihough, R., C. Finn, and R. Couch, Klamath-Blue Mountain lineament, Oregon, *Geology*, *14*, 528–531, 1986.

Rogers, G. C., Variation in Cascade volcanism with margin orientation, *Geology*, *13*, 495–498, 1985.

Ryan, M. D., Neutral bouyancy and the mechanical evolution of magmatic systems, Magmatic Processes: Physiochemical Principles, edited by B. O. Mysen, *Spec. Publ. Geochem. Soc.*, *1*, 151–175, 1987.

Sammel, E. A., Results of test drilling at Newberry volcano, Oregon, and some implications for geothermal prospects in the Cascades, *Geotherm. Resour. Counc. Bull.*, *10*(11), 3–8, 1981.

Sammel, E. A., and S. Benson, An analysis of the hydrologic effects of proposed test drilling in the Winema National Forest near Crater Lake, Oregon, *Trans. Geotherm. Resour. Counc.*, *11*, 293–303, 1987.

Sammel, E. A., S. E. Ingebritsen, and R. H. Mariner, The hydrothermal system at Newberry volcano, Oregon, *J. Geophys. Res.*, *93*, 10,149–10,162, 1988.

Sherrod, D. R., Geology, petrology, and volcanic history of a portion of the Cascade Range between latitudes 43°–44°N, central Oregon, U.S.A., Ph. D. dissertation, Univ. of Calif., Santa Barbara, 1986.

Sherrod, D. R., and L. G. Pickthorn, Some notes on the Neogene structural evolution of the Cascade Range in Oregon, Geological, Geophysical, and Tectonic Setting of the Cascade Range, edited by L. J. P. Muffler, C. S. Weaver, and D. D. Blackwell, *U.S. Geol. Surv. Open File Rep.*, *89-178*, 351–368, 1989.

Sherrod, D. R., and J. G. Smith, Quaternary extrusion rates of the Cascade Range, Northwestern United State and southern British Columbia, *J. Geophys. Res.*, this issue.

Simpson, R. W., R. C. Jachens, R. J. Blakely, and R. W. Saltus, A new isostatic residual gravity map of the conterminous United States with a discussion on the significance of isostatic residual anomalies, *J. Geophys. Res.*, *91*, 8348–8372, 1986.

Smith, R. L., and H. R. Shaw, Igneous-related geothermal systems, Assessment of Geothermal Resources of the United States—1975, edited by D. E. White and D. L. Williams, *U.S. Geol. Surv. Circ.*, *726*, 53–83, 1975.

Stanley, W. D., W. D. Mooney, and G. S. Fuis, Deep crustal structure of the Cascade Range and surrounding regions from seismic refraction and magnetotelluric data, *J. Geophys. Res.*, this issue.

Steele, J. L., D. D. Blackwell, and J. H. Robison, Heat flow in the vicinity of the Mt. Hood volcano, Oregon, Geology and Geothermal Resources of the Mt. Hood Area, Oregon, edited by G. R. Priest and B. F. Vogt, *Spec. Pap. Oreg. State Dep. Geol. Miner. Ind.*, *14*, 31–42, 1982.

Swanberg, C. A., and J. Combs, Geothermal drilling in the Cascade Range: Preliminary results from a 1387-m core hole, Newberry volcano, Oregon, *Eos Trans. AGU*, *67*, 578–580, 1986.

Swanberg, C. A., W. C. Walkey, and J. Combs, Core hole drilling and the "Rain Curtain" phenomenon at Newberry Volcano, Oregon, *J. Geophys. Res.*, *93*, 10,163–10,173, 1988.

Talwani, M., and M. Ewing, Rapid computation of gravatational attraction of three-dimensional bodies of arbitrary shape, *Geophysics*, *25*, 203–225, 1960.

Taylor, E. M., Roadside geology, Santiam and McKenzie Pass Highways, Oregon, Andesite Conference Guidebook, edited by H. M. Dole, *Bull. Oreg. Dep. Geol. Miner. Ind.*, *62*, 3–34, 1968.

Taylor, E. M., Volcanic history and tectonic development of the central High Cascade Range, Oregon, *J. Geophys. Res.*, this issue.

Verplanck, E. P., and R. A. Duncan, Temporal variation in plate convergence and eruption rates in the Western Cascades, Oregon, *Tectonics*, *6*, 197–209, 1987.

Walker, G. E., Geology of the High Lava Plain province, *Bull. Oreg. Dep. Geol. Mineral. Ind.*, *64*, 77–79, 1969.

Weaver, C. S., and G. E. Baker, Geometry of the Juan de Fuca plate beneath Washington from seismicity and the 1949 South Puget Sound earthquake, *Bull. Seismol. Soc. Am.*, *78*, 264–275, 1988.

Weaver, C. S., and S. D. Malone, Overview of the tectonic setting and recent studies of eruptions of Mount St. Helens, Washington, *J. Geophys. Res.*, *92*, 10,149–10,155, 1987.

Wells, R. E., Paleomagnetic rotations and the Cenozoic tectonics of the Cascade arc, Washington, Oregon, and California, *J. Geophys. Res.*, this issue.

Williams, D. L., and R. P. Von Herzen, On the terrestrial heat flow and physical limnology of Crater Lake, Oregon, *J. Geophys. Res.*, *88*, 1094–1104, 1983.

Ziagos, J. P., and D. D. Blackwell, A model for the transient temperature effects of horizontal fluid flow in geothermal systems, *J. Volcanol. Geotherm. Res.*, *27*, 371–397, 1986.

G. L. Black and G. R. Priest, Department of Geology and Mineral Industries, 905 State Office Building, Portland, OR 97201.

D. D. Blackwell and J. L. Steele, Department of Geological Sciences, Southern Methodist University, Dallas, TX 75275.

M. K. Frohme, CERI, Memphis State University, Memphis, TN 38152.

C. F. Murphey, Union Pacific Resources, 1817 Mossy Oak St., Arlington, TX 76012.

(Received August 10, 1989;
revised July 13, 1990;
accepted July 20, 1990.)